Composites Part C: Open Access 4 (2021) 100099

Contents lists available at ScienceDirect

Composites Part C: Open Access

journal homepage: www.elsevier.com/locate/jcomc

Experimental calibration of the bond-slip relationship of different CFRP-to-timber joints through digital image correlation measurements

Hugo C. Biscaia [a,*], Raquel Almeida [b], Shishun Zhang [c], João Canejo [d]

[a] UNIDEMI and Department of Mechanical and Industrial Engineering, Faculdade de Ciências e Tecnologia, Universidade Nova de Lisboa, Caparica 2829-516, Portugal
[b] UNIDEMI and Department of Mechanical and Industrial Engineering, Faculdade de Ciências e Tecnologia, Universidade Nova de Lisboa, Caparica 2829-516, Portugal
[c] School of Civil and Hydraulic Engineering, Huazhong University of Science and Technology, China
[d] CENIMAT/i3N and Department of Materials Science, Faculdade de Ciências e Tecnologia, Universidade Nova de Lisboa, Caparica 2829-516, Portugal

ARTICLE INFO

Keywords:
DIC technique
CFRP laminates
Timber
Bond-slip
Closed-form solutions

ABSTRACT

Nowadays, the use of the Digital Image Correlation (DIC) technique has spread and it is being used in several engineering areas to measure displacements. The available data obtained from the DIC measurement to evaluate the bond performance between a Carbon fibre Reinforced Polymer (CFRP) externally bonded to a timber substrate is scarce. From the existing data obtained with other materials, this contactless technique revealed to be quite useful but its accuracy with other well-established techniques, such as the use of electric strain gauges is not well understood yet. Therefore, the current work aims to study the accuracy of 2D DIC measurements with the measurements obtained from the use of strain gauges within a low-cost perspective. To that end, several CFRP-to-timber bonded joints were tested under the single-lap shear test and different bonding techniques were considered as well. Some flaws intrinsically derived from the DIC measurements that complicate the bond assessment, such as the fluctuations in the generated displacements field, are identified, and to bypass this problem a new methodology is proposed. This new methodology is based on two different closed-form solutions that, after defining the local and global bond behaviours of different CFRP-to-timber bonded joints, allowed to eliminate the fluctuations found from the DIC measurements, facilitating the estimation and the comprehension of the full debonding process of the CFRP-to-timber joints, which was achieved with a good proximity to the homologous debonding process derived from the strain gauge measurements.

1. Introduction

Recently, adhesively bonded structures have gained some focus rather than other joining techniques. With the use of an adhesive instead of, *e.g.*, welding or introducing metallic fixations, no residual stresses are introduced into the bonded elements and it avoids stress concentrations without increasing the weight of the bonded materials [1–3]. However, the main issue of such bonded structures is the premature debonding inherent to such technique, *i.e.* the bond failure of the structure when the rupture of the bonded materials is still far away of being reached. Therefore, and depending of the situation under analysis, it is usual to adopt different and improved bonding techniques that aimed to delay or even prevent that premature debonding. A key aspect of the analysis of the debonding process of an adhesively bonded structure is the identification of the local bond-slip relationship. In the case of Carbon fibre Reinforced Polymers (CFRP) bonded to a timber element, scarce information is available in the literature, *e.g.* [4–9]. Nevertheless, some authors have come to the conclusion that the experimental results could be mathematically approximated to different types of local bond-slip relationships, such as bi-linear [10], trilinear [11, 12] or exponential [13–16] functions. Such a variety of proposals may be due to the fact that several timber species exist all around the world which makes difficult to find a consensual bond-slip model. Furthermore, in some of those studies [11–13], the timber provenience was from an ancient building from the 19th century that was demolished [17] and the timber used to study the advantages of using CFRP laminates to flexurally repair old timber pavements.

In the majority of the cases, the local bond-slip relationships are experimentally obtained from the use of the strain gauges that are bonded onto the CFRP composites and throughout the bonded length of the CFRP-to-timber joints. This is a well- established monitoring technique, however, with the improvement of digital cameras at a relative low cost, the use of other contactless techniques capable of monitoring displacements, such as the Digital Image Correlation (DIC), have risen recently. Unlike the strain gauges, the DIC technique allows us to measure a continuous displacement field developed within an area (or surface) of interest. To that end, the DIC technique compares digital images before

* Corresponding author.
E-mail address: hb@fct.unl.pt (H.C. Biscaia).

https://doi.org/10.1016/j.jcomc.2020.100099
Received 16 November 2020; Accepted 28 December 2020

and after a deformation and it traces the displacements of small subsets (or facets) of the area of interest. This tracing process is possible if the area of interest is painted with a speckle pattern paint that will allow the generation of several subsets with a unique distribution of different pixels with different grey levels. However, it is usually reported in the literature [18–21] that the generated displacement fields show irregular displacements distributions, *i.e.* show several peak and valleys, that may difficult the analysis of the interfacial bond stresses developed within the bonded joint.

Zhu et al. [18] used the 2D DIC technique to measure the displacements of FRP sheets bonded onto concrete blocks. The typical global load-slip behaviours of the double-lap shear specimens were characterized by an initial linear stage followed by a nonlinear one that stabilized at a plateau corresponding to the debonding load. The DIC measurements were quite accurate with those obtained from the strain gauges but during the nonlinear stage of the load-slip relationship the DIC technique provided smaller slips than those calculated from the strain gauges. The generated strain measurements showed several peak and valleys throughout the bonded length which would complicate the evaluation of the bond characteristics between the FRP sheets and the substrate, if the authors [18] would not have used an analytical expression from the literature [22] to smooth the FRP strains. For that, a fitting process was proposed and an exponential bond-slip relationship was determined. When compared with the results provided by the strain gauges, the typical bond-slip relationships obtained by the fitting process revealed higher maximum bond stresses with a less smoother and softening decay after that.

A similar approach was followed by Yuan et al. [19] where an analytical expression was used to smooth the significant irregularities determined from the DIC measurements of Basalt (B) FRP strains bonded to a concrete substrate. Based on that analytical expression that tracked the BFRP strains throughout the bonded length, the authors [19] have derived the slips and the bond stresses to estimate the local bond-slip relationship.

The complexity of the debonding phenomena between an FRP composite and a concrete substrate was discussed by Czaderski et al. [20] who used the Stereo DIC technique to prove that the shear-lap single tests cover not only the fracture Mode II, as it would be initially expected, but also has displacements consistent with fracture Mode I, *i.e.* perpendicular with the bonded area, probably due to the influence of the aggregates in the concrete substrate. Therefore, they claimed that the use of single-lap shear tests does not induce a pure Mode II fracture into the specimens but a Mixed Mode (*I*+II) instead. Although the fluctuations of the DIC measurements were not meaningful, the authors [20] also used a fitting process to smooth the DIC measurements and obtain well-defined slip, CFRP strain and bond stress configurations.

Similarly, Martinelli et al. [21] have come to the same conclusion using the 3D DIC technique. In this case, the authors [21] have proposed a numerical strategy to predict the debonding between CFRP composites and a concrete substrate under a Mixed Mode fracture process. The 3D DIC technique and the numerical results seemed to agree very well.

Other works can be found in the literature dealing with the bond evaluation between CFRP or Textile Reinforced Mortars (TRM) composites and clay bricks [23–27] or between CFRP and steel bars [28,29] through the use of the DIC technique. In none of these works, the DIC technique seemed to fail and a high precision of the experiments was always claimed by all.

As it was demonstrated, the DIC technique is a well accepted and extensively used technique but, to the best knowledge of the authors, no information exists about how accurate the DIC measurements can be when compared with other well-established monitoring techniques was carried out so far. Moreover, it was not used to evaluate the bond characteristics between a CFRP laminate and a timber substrate under different bonding conditions. To mitigate that gap in the actual literature, this work aimed to the use of the 2D DIC technique in order to capture the full-field displacements of CFRP-to-timber bonded joints when monotonically subjected to the single-lap shear test. The generated DIC measurements are reported and a brief comparison with the results obtained from the use of strain gauges are presented as well. The weaknesses of such approach on the evaluation of the debonding process of CFRP-to-timber joints are shown and an alternative and new methodology is proposed to bypass those flaws. This new proposal consists on the development of a fitting process that aims to the definition of the local bond-slip relationship from the DIC results. Since the use of electric strain gauges is a well-established monitoring technique, the DIC results are confronted against the homologous results determined from the strain gauge measurements. To validate the applicability of the proposed method, different bonding techniques were applied to a total of 30 single-lap shear specimens, with and without the installation of a mechanical anchorage at the CFRP unpulled end. In some single-lap shear specimens, the 2D DIC technique failed to measure part of the generated displacement fields after the debonding of the anchored CFRP-to-timber joints was reached. Nevertheless, this revealed to be not a real flaw since the evaluation of the CFRP-to-timber bonded joints through the application of the proposed methodology requires the definition of the local bond-slip relationship, which is obtained until the debonding load, and until then, no displacements were missed by the DIC technique. Globally, when the results were compared with those provided by the strain gauges, no meaningful differences were found.

2. Experimental program

2.1. Details of the pull-out specimens

Two different groups of CFRP-to-timber bonded joints were adopted. In the first group, the bonded joints were free of any mechanical anchorages whilst the second group a mechanical anchorage was installed at the CFRP unpulled end. In the first group, two different bonding techniques were considered: the Externally Bonded Reinforcement (EBR) and the EBR On Grooves (EBROG) bonding techniques. Therefore, two series are included in this group which, depending of the CFRP thickness (t_f), are denoted as GIS1a (if $t_f = 1.4$ mm) or GIS1b (if $t_f = 2.8$ mm). The other series in this first group is denoted as GIS2 (see Table 1).

In the second group, the specimens were divided into five series. The first series considered the use of CFRP spike anchors. However, to analyse the influence of the number of CFRP spike anchors on the CFRP-to-timber bond performance, the first series contemplated the use of 2 or 3 spike anchors distanced 150 and 75 mm between them, respectively. If in this mechanical anchorage 2 CFRP spike anchors were used, then the ID of the specimens is GIIS1a but if not, the ID of the specimens is GIIS1b instead. The second series of this group (GIIS2) consisted on the insertion of an inverted small metallic profile with a U-shape into the timber substrate. The GIIS3 specimens are characterized by the installation of a steel plate which is externally pressed against the CFRP laminate and fixed with steel bolts to the timber substrate. The next series (GIIS4) consisted on the use of a rectangular profile to guide the CFRP laminate into the core of the timber prism. This small profile is made of aluminium and it was inserted into the timber with a rotation of approximately 15° with the vertical axis and fixed to the timber substrate with metallic screws. The mechanical anchorage used in the fifth series consisted in embedding the CFRP unpulled end into the timber prism. Since two different CFRP thicknesses were used in this particular series, the specimens were divided into GIIS5a ($t_f = 1.4$ mm) and GIIS5b ($t_f = 2.8$ mm) series. It should be mentioned also that per each series, three shear pull-out specimens were conceived and tested which, from hereafter, the number of the test is added to the ID of the specimen. For instance, the first and third specimens tested on series GIIS1a will be designated as GIIS1a-01 and GII1a-03, respectively. Table 1 summarizes the details of the two groups of shear pull-out specimens under study whilst Fig. 1 shows the aspects of all them before testing.

The shear pull-out specimens consisted on timber prisms with a cross-sectional area of 100 × 70 mm (width × thickness) and a height of

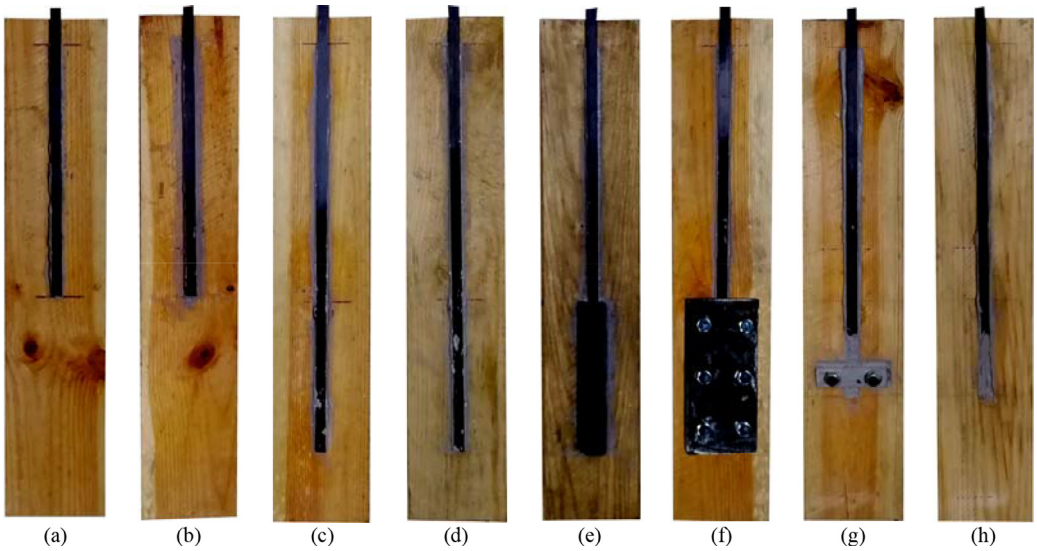

Fig. 1. Overview of the specimens of each series: (a) GIS1a or GIS1b; (b) G1S2; (c) GIIS1a; (d) GIIS1b; (e) GIIS2; (f) GIIS3; (g) GIIS4; and (h) GIIS5a or GIIS5b.

500 mm according to which a CFRP laminate is bonded to. At the front of the specimens (*i.e.* on the top of the specimens shown in Fig. 1) a gap of 25 mm was left unbonded in order to avoid high stress concentrations at this region during the shear pull-out tests. The bond length (L_b) of the specimens were all kept the same, *i.e.* L_b = 250 mm. However, in the anchored CFRP-to-timber bonded joints (*i.e.* in Group II), the specimens had another 150 mm where the anchorages were installed. For instance, the steel plate of GIIS3 (see Fig. 1f) had a length of 150 mm as well. However, it should be mentioned that in the case of the GIIS4 specimens (see Fig. 1g) such extra bonded length was not considered and the CFRP unpulled end ended within the rectangular hollowed profile. On the other hand, embedded lengths of 150 mm long of the CFRP unpulled ends of the GIIS5a and GIIS5b specimens (see Fig. 1h) were inserted into the core of the timber.

2.2. Mechanical properties of the materials

2.2.1. Timber

The timber was supplied from a local supplier who had no information about its mechanical characteristics. Thereby, it was necessary to carry out several tests to identify the mechanical properties of the timber and, based on those results, identify the timber's species. To that end, the following tests were considered: (i) 3-point bending tests; (ii) uniaxial compression tests; and (iii) pull-off tests.

From the first tests, a total of twelve specimens with the dimensions of 20 × 20 × 340 mm (width × thickness × length) were performed. These specimens were conceived without knots to avoid the influence of the results as it is recommended by the Portuguese Standard NP 619 [30]. The grain of the timber was kept parallel to the length of the specimens which allowed us to calculate the strength of the timber parallel to its grain ($f_{wt,0}$). Thus, the tensile strength parallel to the grain of the timber (f_{wt},0) was calculated according to:

$$f_{wt,0} = \frac{3}{2} \cdot \frac{P \cdot L}{b_w \cdot {t_w}^2} \tag{1}$$

whereas the rupture strain (ε_{wt},0) was determined as follows:

$$\varepsilon_{wt,0} = 6 \cdot \frac{\delta \cdot t_w}{L^2} \tag{2}$$

where P is the load applied to the specimen; L is the span of the beam; b_w and t_w are, the width and thickness of the timber, respectively; and δ is the mid span displacement. From Eqs. (1) and (2), the mean tensile strength of the timber was found to be $f_{wtm,0}$ = 104.3 MPa (Coefficient of Variation, CoV = 10.2%) and the mean rupture strain ε_{wtm} = 1.10% (CoV = 12.5%). The Young modulus of the timber was obtained from the slope of a limited part of the stress-strain relationship between 20% and 80% of $f_{wt,0}$. Therefore, the calculated mean Young modulus of the timber is $E_{wtm,0}$ = 12.93 GPa (CoV = 13.1%).

For the characterization of the timber under uniaxial compression, thirteen specimens free of knots with the dimensions of 20 × 20 × 60 mm (width × thickness × length) were carried out according to the Portuguese Standard NP 618 [31]. The grains of the timber and the applied load had the same vertical direction. Based on the results obtained in this compression test, the mean compression strength ($f_{wcm,0}$) and the mean rupture strain (ε_{wcm}) of the timber are 59.26 MPa (CoV = 10.6%) and 3.11% (CoV = 24.2%), respectively. The Young modulus was obtained from the stress-strain relationship by limiting the stress-strain curve to 10% and 40% of $f_{wc,0}$ which led to a mean Young modulus of E_{wcm} = 4.80 GPa (CoV = 25.1%).

The tensile strength of the timber parallel and perpendicular to the grain was also considered by performing twenty pull-out tests. These tests consisted to externally bond a metallic doll with a 50 mm-diameter onto the timber's surface previously cut with a holesaw with an internal diameter of 50 mm as well. The cut in the timber had approximately 20 mm-deep. The metallic dolls were then bonded to the timber's surface through the use of S&P 220 HP resin which was the same resin used to bond the CFRP laminates onto the timber prism. Ten metallic dolls were bonded onto the surface in order to align the load and the timber's grain with the same direction whereas the other ten, the pulling load and the timber's grain had a perpendicular direction. The tests revealed that the mean strength of the timber perpendicular to the grains is $f_{wtm,p,90}$ = 3.23 MPa (CoV = 3.3%). However, in the other direction, *i.e.* with the pull-out force parallel to the timber's grain, the interfacial failure between the metallic doll and the adhesive was always observed. Therefore, and taking into account that the maximum value obtained from these tests was 8.51 MPa, this was assumed as the minimum value of the timber's strength when the load is parallel to its grain ($f_{wt,p,0}$).

It should be mentioned also that the moisture content of the specimens was also measured. For that purpose, the moisture content of twelve specimens randomly selected from the shear pull-out tests and five measurements were made per each specimen. A total of sixty measurements were then carried out which provided an average moisture content of the timber of 16.4% (CoV = 15.7%).

Finally, and considering all these results, the Portuguese guidelines M1 and M4, provided by the Portuguese National Laboratory of Civil Engineering [32, 33], suggest that the timber used in this work is a

Table 1
Details of the shear pull-out specimens.

Group	Series	ID	Bonding technique	Anchorage type
I (with no anchorages)	1a	GIS1a-01 to 03	EBR with a CFRP thickness (t_f) of 1.4 mm.	None
	1b	GIS1b-01 to 03	EBR with a CFRP thickness (t_f) of 2.8 mm.	None
	2	GIS2–01 to 03	EBR On Grooves (EBROG) - groove of 6 mm wide and 40 mm deep.	None
II (with an anchorage)	1a	GIIS1a-01 to 03	EBR with a CFRP thickness (t_f) of 2.8 mm.	2 CFRP spike anchors with 100 mm space between them.
	1b	GIIS1b-01 to 03		3 CFRP spike anchors with 50 mm space between them.
	2	GIIS2–01 to 03		2 superposed L-shaped metallic profiles with a length of 150 mm.
	3	GIIS3–01 to 03		Steel plate with 20 × 70 × 150 mm (thickness × width × length).
	4	GIIS4–01 to 03		Embedded rectangular hollowed profile .
	5a	GIIS5a-01 to 03	EBR with a CFRP thickness (t_f) of 1.4 mm.	CFRP free end embedded into the cross-sectional area of the timber.
	5b	GIIS5b-01 to 03	EBR with a CFRP thickness (t_f) of 2.8 mm.	

Scots Pine (*Pinus sylvestris* L.), with a corresponding C50 strength class and an average density of 550 kg/m^3 [34].

2.2.2. CFRP laminate

Two different CFRP laminates with the same width of b_f = 10 mm but with two different thicknesses (t_f) of 1.4 and 2.8 mm were used in this work. To mechanically characterize each CFRP laminate, six tensile tests were carried out. The stress-strain relationships obtained from both CFRP laminates showed a linear behaviour with a fragile rupture. The mean tensile strength (f_{fm}) and rupture strain ($\varepsilon_{fu,m}$) of the CFRP laminate with t_f = 1.4 mm are 2366.4 MPa (CoV = 14.6%) and 1.40% (CoV = 14.5%), respectively. On the other hand, the other thicker CFRP laminate revealed a mean tensile strength and rupture strain values of 2158.9 MPa (CoV = 4.0%) and 1.35% (CoV = 4.8%), respectively. The calculated mean Young modulus (E_{fm}) of the thinner CFRP laminate was 169.3 GPa (1.4%) whereas in the CFRP laminate with t_f = 2.8 mm the corresponding calculated mean Young modulus is 159.6 GPa (2.6%).

2.2.3. Adhesive

The adhesive used in this work was the epoxy resin S&P220 HP which was supplied from a local S&P fabricant. This resin is a bi-component epoxy resin that before used to bond the CFRP laminated onto the timber substrate, a mixture of two components should be made first. The component A of the resin is the epoxy resin whilst the component B is the hardener. The former one has a light grey colour whereas the latter has a dark coloured aspect and when mixed according to the ratio 2:1 in weight (resin:hardener), as recommended by the S&P fabricant, has a final grey and homogeneous colour aspect. Under these conditions, the fabricant ensures that the adhesive should has a minimum tensile strength ($f_{pt,\min}$) of 15.0 MPa and a Young modulus (E_{pt}) greater than 7.10 GPa. However, considering the experiments carried out by Carvalho [35] with the same resin supplied by the same local S&P fabricant, the corresponding tensile strength and the rupture strain of the resin were found to be f_{pt} = 29.0 MPa and ε_{pt} = 3.65%, respectively.

2.3. Procedures followed for the DIC measurements

The DIC measurement is a contactless and optic technique that uses the mathematical correlation method to analyse different digital pictures that were taken from a specimen during a test period. This technique has been improving and many engineering problems have been reported in the literature [36–40] as examples of high precision found from mono or stereo DIC supported measurements. So, bearing in mind that the DIC measurements will be compared with another conventional measurement technique such as the electric strain gauges, the procedures undertaken during the experimental program are described next in more detail. Hence, eight strain gauges were bonded throughout the bonded length of each shear pull-out specimen with a regular distance between them of approximately 34.3 mm. This distance allowed us to use a sufficient number of strain gauges without losing precision on the evaluation of the bond performance of FRP-to-parent material bonded joints as suggested in the literature [41, 42].

For the DIC measurements, an area of interest was created on the bonded side of the shear pull-out specimens with a spray paint with a granite aspect. The area of interest comprehended the bonded length of the shear pull-out specimens and the width of the timber prism. The spray paint produced a speckle pattern aspect with several dark and light points randomly distributed throughout the full area of interest. The displacements of these points were captured by a digital camera with a maximum resolution of 5184 × 3456 pixels. The digital camera was fixed to a steel frame which ensured that the differences between images were caused by the pull-out load transmitted to the CFRP laminate. Several photos were taken at a regular interval of 5 s of the test duration. Moreover, to prevent any light interferences (*e.g.* shadows from the surrounding equipment) on the adopted area of interest, an artificial

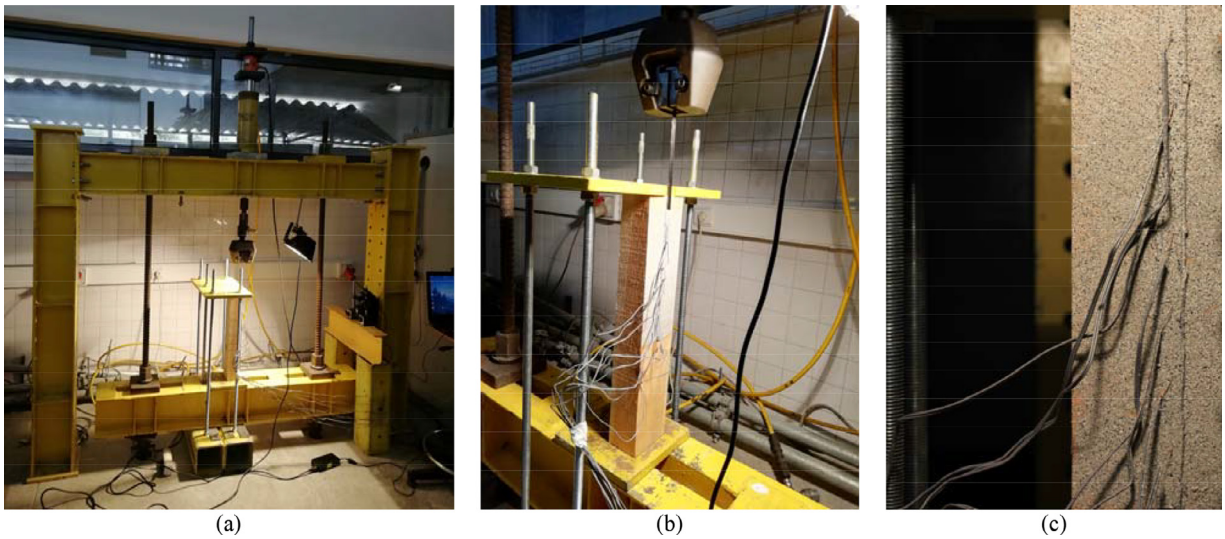

Fig. 2. Overview of the shear pull-out tests: (a) test setup; (b) detail of the shear pull-out specimen inside the steel frame; and (c) picture taken with the digital camera (overview of the spaying aspect).

spotlight with 100 W was used. Fig. 2a and 2b shows an overview of the test setup as well as the area of interest created for the DIC measurements. In Fig. 2c it is also possible to observe the aspect of the speckle pattern created by the spray paint.

It was expected that the shear pull-out tests carried out in this work would induce deformations in a plane parallel to the digital camera. No meaningful deformations in the perpendicular direction are expected to occur and therefore, the 2D DIC method and the latest free version of GOM Correlate software [43] were used to measure the displacements of the CFRP laminate (u_f) and the timber (u_w). The measurement process begins with the first picture which has no deformations and it is used to calibrate and define the scale of the measurements. The area of interest of this first picture is mapped by correlation windows (or facets), within which an independent measurement of displacement is calculated. However, it is important to mentioned that if a too excessive detailed deformation mapping of the area of interest is assumed, then the originated displacements fields will have relevant peaks and valleys that compromise the bond assessment between an FRP composite and a parent material substrate [18, 39, 40]. Thereby, a standard facet size of 76 × 76 pixels with 60 pixels distance was used in the DIC measurements of all shear pull-out specimens. The distance between the camera and the timber's painted surface was approximately 550 mm and a conversion factor of approximately 50 μm/pixel was obtained for all the shear pull-out tests. These conditions led to a typical resolution of the displacement measurements that ranged from 0.01 to 0.02 mm.

To illustrate the results obtained from the DIC technique, Fig. 3 shows the displacements obtained from specimen GIS1a-01 at five different stages of its load-slip response. At the same time, the range of displacements measured within the area of interest of the specimen is also shown. It should be mentioned that the slip measures the relative displacement between the CFRP laminate and the timber substrate. These particular results show higher displacements (here with negative signal since the vertical axis and the displacements have opposite directions) closed to the CFRP pulled end. In the opposite, the regions closest to the CFRP free end have the lowest values (here with positive values due to the same direction of the y coordinate and the displacements). Such differences are accentuated as the load transmitted to the CFRP laminate increase. It is also visible that the displacements in the timber closed to the CFRP loaded end have positive signal which is attributed to the compressions imposed by the reaction steel plate placed at the top of the specimen (see Figs. 2a or 2b) to the timber prism.

Since the DIC software does not calculate relative displacements between two selected materials, the methodology already used by the authors in other works and available in the literature [39, 40] was also adopted here. So, from the displacements of the CFRP laminate and from the timber, two vertical lines were created throughout the area of interest, one throughout the CFRP laminate and another one throughout the timber surface. Then, twenty-five points distanced between them 10 mm (same as the length of the strain gauges) were created and the corresponding displacements during the test period saved. The relative displacements (or slips) were then calculated by coupling both results at the same distance from the CFRP free end, *i.e.*:

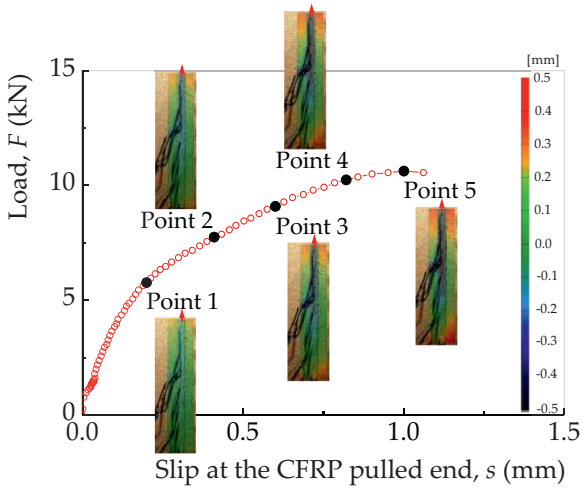

Fig. 3. Displacements of the area of interest obtained from the DIC measurement at five different points of the load-slip response of specimen GIS1a-01.

$$s(y_i) = u_f(y_i) - u_w(y_i) \tag{3}$$

where $u_f(y_i)$ and $u_w(y_i)$ are the displacements in the CFRP laminate and in the timber measured at point y_i, respectively.

3. Experimental results

3.1. Loads and failure modes

From the experiments, the debonding (F_{deb}) and the ultimate (F_{ult}) loads of all specimen series were identified. Since the specimens in the first group had no mechanical anchorage installed at the CFRP unpulled

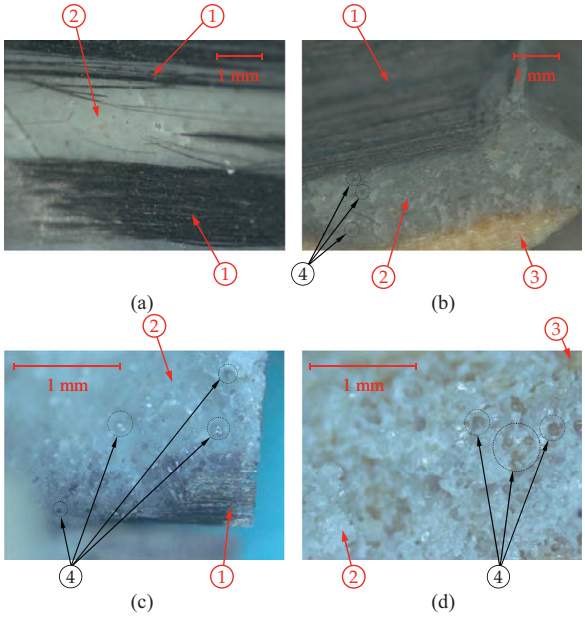

Fig. 4. Amplified views of the adhesive failure mode between the adhesive and the CFRP laminate occurred in specimens: (a) GIIS2–03; (b) GIS2–02; (c) GIIS3–01; and (d) GIIS2–02.

end, the debonding and the ultimate loads in specimen series GIS1a, GIS1b and G1S2 have the same value. Nevertheless, the CFRP spike anchors used in GIIS1b specimen series have not influenced the strength of the CFRP-to-timber joint and consequently, the debonding and ultimate loads are the same. It should mentioned that in specimen series GIIS1a only the third specimen (GIIS1a-03) registered an increase of the ultimate load (21.76 kN) from the debonding load (17.88 kN) of 21.7%. In all the remaining specimen series the ultimate load is higher than the debonding load. In terms of average values, Table 2 summarizes these results, which are completed with the failure modes observed from the tested specimens.

The highest ultimate load reached in the shear pull-out specimens was 38.33 kN, which was achieved with the use of two superposed L-shaped metallic profiles as a mechanical anchorage. Still, this value is quite far from the rupture load of the CFRP laminate. Although the average ultimate load calculated for the specimens in GIIS5a is not within the first three highest values, 26.28 kN corresponds to approximately 80.9% of the rupture load of the CFRP laminate with t_f = 1.4 mm.

The failure modes observed from the different tested specimens varied between specimens and, in the GIIS5a series, the three tested specimens exhibited three distinguished failure modes. Nevertheless, the interfacial failure modes within the timber and the adhesive or within the adhesive and the CFRP laminate were the ones most clearly observed. Still, in some specimens, the rupture of the timber substrate was also observed (*e.g.* GIIS1a-03, GIIS4–02 or GIIS5a-03), whilst the rupture of the adhesive was observed in specimen series GIS2 and in the specimen GIIS2–02.

After the mechanical testing of the pull-out specimens, small samples were removed from the ruptured surfaces in order to observe them through a Digital Stereo Microscope (DSM) equipped with a 10 MP digital camera. Although in some cases the CFRP laminates debonded from the adhesive (adhesive failure mode between the adhesive and the CFRP laminate), Figs. 4a to 4c show three examples where some carbon fibres were still bonded to the adhesive after testing. The rupture of several carbon fibres can be also seen in Fig. 4a. Also, Fig. 4c shows the failure mode observed from the CFRP laminate side of specimen GIIS3–01, whilst Fig. 4d shows the failure mode observed from the timber sub-

Table 2
Average values of the debonding and ultimate loads.

ID	Debonding load, F_{deb} (kN)	Ultimate load, F_{ult} (kN)	Failure modes
GIS1a-01 to 03	12.65	12.65	Timber/Adhesive (in GIS1a-01) and Timber/Adhesive + Adhesive/CFRP
GIS1b-01 to 03	15.05	15.05	Timber/Adhesive + Adhesive/CFRP
GIS2–01 to 03	24.38	24.38	Adhesive + Adhesive/CFRP
GIIS1a-01 to 03	16.76	18.05	Timber/Adhesive + Adhesive/CFRP and Timber/Adhesive + Timber (in GIIS1a-03)
GIIS1b-01 to 03	18.95	18.95	Timber/Adhesive + Adhesive/CFRP
GIIS2–01 to 03	16.46	38.33	Timber/Adhesive + Adhesive/CFRP and Adhesive (in GIIS2–02)
GIIS3–01 to 03	18.50	23.95	Timber/Adhesive + Adhesive/CFRP
GIIS4–01 to 03	16.86	27.15	Timber/Adhesive (in GIIS4–01), Timber/Adhesive + Timber (in GIIS4–02) and Timber/Adhesive + Timber + Adhesive/CFRP (in GIIS4–03)
GIIS5a-01 to 03	14.40	26.28	Timber/Adhesive (in GIIS5a-01), Timber/Adhesive + Timber (in GIIS5a-02) and Timber/Adhesive + Timber + Adhesive/CFRP (in GIIS5a-03)
GIIS5b-01 to 03	19.86	29.05	Timber (in GIIS5b-01) and Timber/Adhesive + Adhesive/CFRP

strate side of specimen GIIS2–02. Despite mixing the two components (A and B) of the resin manually for at least 10 min without allowing the air into the mixture, Figs. 4b to 4d show small air voids across the thickness (see Fig. 4b) and width (see Figs. 4c and 4d) of the adhesive. This is a relevant point that should be carefully considered during the preparation of the resin because excessive formation of air voids will reduce the strength of the adhesive and could compromise the final performance of the CFRP-to-timber bonded joints. Fig. 4b also shows no rupture between the timber substrate and the resin, which means that good compatibility between these two elements was achieved in this bonded region.

3.2. Precision of the DIC measurements

To compare the measurements carried out by the DIC technique with those from the strains gauges bonded on the CFRP laminates, it is first necessary to explain how the slips were determined from the latter measurements. Therefore, based on the measurements of eight strain gauges bonded along the bonded length, the slips (s) can be calculated according to following expression [44, 45]:

$$\frac{ds}{dy} = (1+\beta)\cdot\varepsilon_f \tag{4}$$

where β stands for the ratio between the axial stiffness of the CFRP laminate and the timber substrate as follows:

$$\beta = \frac{E_f b_f t_f}{E_w b_w t_w} \tag{5}$$

where E_f, b_f and t_f are the Young modulus, the width and the thickness of the CFRP laminate, respectively; E_w, b_w and t_w are the Young modulus, the width and the thickness of the timber substrate, respectively. Integrating Eq. (4) and solving it numerically, it yields:

$$s(y_{i+1}) = (1+\beta)\int_{y_i}^{y_{i+1}} \varepsilon_f dy + s(y_i) \approx (1+\beta)\cdot\left(\varepsilon_{f,i+1}+\varepsilon_{f,i}\right)\cdot\frac{y_{i+1}-y_i}{2} + s(y_i) \tag{6}$$

where $s(y_i)$ and $s(y_{i+1})$ are the slips at point y_i and y_{i+1}; $\varepsilon_{f,i}$ and $\varepsilon_{f,i+1}$ are the axial strains in the CFRP laminate at points y_{i+1} and y_i, respectively.

3.2.1. Global slip during the test period

Fig. 5 shows the global slips obtained from both measurements at the CFRP pulled end during the test period. In the Figs. 5a to 5c, the slips obtained during the test period correspond to the specimens within Group I (free of any mechanical anchorages), whilst the slips observed in Figs. 5d to 5j correspond to the specimens of Group II (with a mechanical anchorage). The accuracy of the DIC measurements with the results obtained from Eq. (6) is evaluated by the calculation of the Integral Absolute Error (IAE), which is sensitive to the deviation of a theoretical result and is commonly used for model assessment [46]:

$$IAE = \sum_{t=1}^{n} \frac{\left|{s_{0,t}}^{DIC} - s_{0,t}\right|}{\sum_{t=1}^{n}\left|{s_{0,t}}^{DIC}\right|} \tag{7}$$

where ${s_{0,t}}^{DIC}$ and $s_{0,t}$ correspond to the slips measured by the DIC technique and those calculated from the strain gauges at the CFRP pulled end, *i.e.* using Eq. (6), at the instant t of the test period, respectively; and n corresponds to the number of measurements carried out during the test period.

The Absolute Deviation (AD) and the Mean Absolute Deviation (MAD) were also calculated as follows:

$$AD_{,t} = \left|{s_{0,t}}^{DIC} - s_{0,t}\right| \tag{8}$$

and

$$MAD = \frac{1}{n}\times\sum_{t=1}^{n}\left|{s_{0,t}}^{DIC} - s_{0,t}\right|. \tag{9}$$

A general overview of the global slip *vs.* duration of the test is shown in Fig. 5, where it can be observed that the use of the DIC technique provided very close results to those determined from the strain gauges, especially until the debonding load of the specimens was reached. However, in some anchored CFRP-to-timber specimens, *i.e.* in the second group of specimens, once the debonding load was reached, the DIC technique was not able to track some points (or facets) of the CFRP laminate anymore. In other specimens, such as GIIS3–01 and GII5a-03, the DIC technique overestimated the global slips after the CFRP debonding. However, in those specimens where the global slips could not be measured with the DIC technique, the global slips were obtained by the axial displacement of the CFRP laminate, as described in the literature [14, 47]. This option allowed us to make other and more complete analyses in the subsequent sections up until the ultimate load. This lack of measurements of the DIC technique was attributed to a sudden displacement increase in the CFRP laminate during the debonding phenomena between the CFRP and the timber substrate that prevented the DIC technique from continuing to monitor the same facet between two consecutive photos (5 s apart). To facilitate the identification of these points, all these were marked with a cross in Figs. 5f to 5j.

In terms of the IAE and AD values, the results revealed that the former did not exceed 35%, whilst the latter had a maximum value of 0.79 mm (in specimen GIIS5a-03). Nevertheless, it should be mentioned that in specimen GIIS1b-01, where the calculated value of IAE was the highest (33.9%), the maximum value of AD reached in this specimen was only 0.07 mm at the ultimate load. On the other hand, despite highest calculated values of AD being in specimen GIIS5a-03 (see Fig. 5i), the calculated value of IAE was 19.0%. It should also be highlighted that IAE values lower than 10% were obtained from several other specimens. Moreover, and within an overall perspective of the calculated values of the MAD, a large majority of the tests had an associated MAD value that ranged between 0.01 to 0.05 mm.

Faced with these quite remarkable results, and taking into account the typical resolution of the DIC measurements, it can be asseverated that the 2D DIC technique applied in this work can be used to evaluate the global bond performance of CFRP-to-timber bond joints, particularly if no mechanical anchorages are used. However, the results do also suggest some prudence is needed with the exclusive use of the 2D DIC technique for anchored CFRP-to-timber bonded joints (*e.g.*, see Fig. 5g).

3.2.2. Global load-slip responses

The characteristics of the global load-slip responses depend on whether the CFRP-to-parent material has a mechanical anchorage installed at the CFRP unpulled end or not. However, whether the mechanical anchorage is used or not, the load-slip responses before the debonding load (F_{deb}) have a similar shape. In other words, until the debonding load is reached, the load-slip relationship has an initial (almost) linear stage, which is followed by a nonlinear one. After that load, the CFRP laminate separates from the timber substrate with a loud sound, which corresponds to one, or to a combination of more than one, of the following situations: rupture of some CFRP fibres, rupture of the adhesive, rupture of a thin layer of the timber substrate or rupture of the CFRP/adhesive and/or adhesive/timber interfaces. Usually, this occurs when the loads transmitted to the CFRP laminates are lower than the rupture load of the CFRP, which is a very well-known drawback of these adhesively bonded joints, described in the literature as premature debonding [48–52].

Although the use of mechanical anchorages does not prevent the above ruptures, it does permit additional loads to be transmitted to the CFRP laminate even after the CFRP composite has detached from the substrate. In this stage, the load-slip response of the CFRP-to-parent material bonded joint tends to another stage with a linear behaviour, which corresponds to the axial and elastic displacement of a finite CFRP length with a length equal to the bonded length of the joint [14, 47].

Fig. 6 shows the load-slip responses obtained from all tested specimens. On the right-hand side of this figure, the AD values obtained

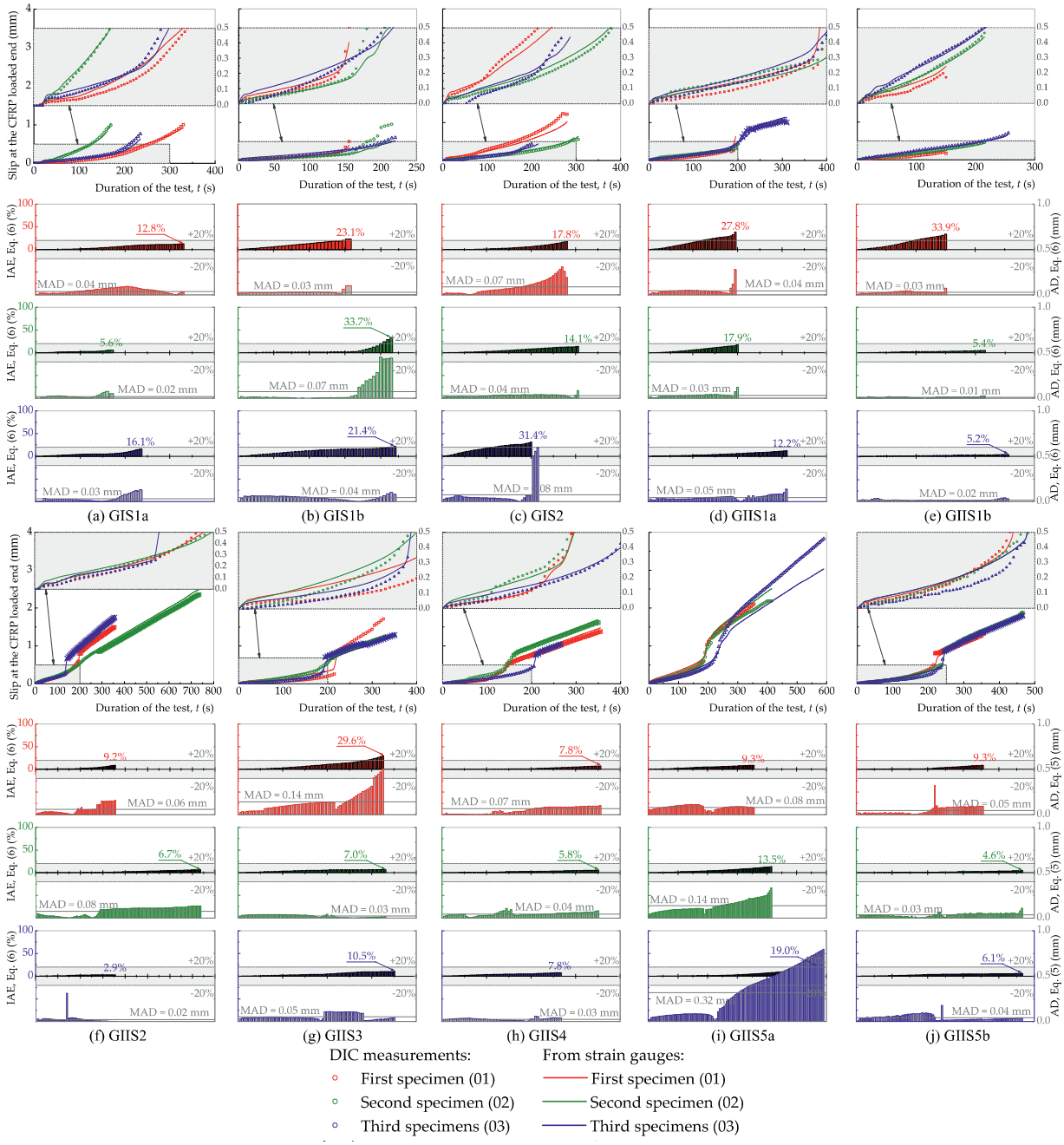

Fig. 5. Comparisons between the slip at the CFRP loaded end during the test period measured by the DIC technique and calculated from the strain gauges.

from each load interval of 5 s during test is shown. At the same time, to calculate the deviation of the DIC measurements from the strain gauge measurements at a specific load magnitude, the Relative Percent Error (RPE) and the Mean Relative Percent Error (MRPE) were also considered. Hence, the RPE is defined according to:

$$RPE_{,t} = 100 \times \frac{s_t{}^{DIC} - s_t}{s_t} \tag{10}$$

whereas the equation used to calculate the MRPE was

$$MRPE = \frac{100}{n} \times \sum_{t=1}^{n} \frac{s_t{}^{DIC} - s_t}{s_t}. \tag{11}$$

The RPE values obtained throughout the test period are shown on the left-hand side of Fig. 6. The results revealed that the RPE tends to be highest when the transmitted load to the CFRP laminate is within the first stage of the load-slip response. Since the loads transmitted to the CFRP laminate in this first stage are low, the AD values can be considered almost marginal. With the load increase, this pattern tended to invert, *i.e.* the RPE values decreased whilst the AD values tended to increase. Nevertheless, and with some exceptions, the RPE values obtained from the tested specimens ranged between the interval of −20% to +20% at the debonded or ultimate loads, whereas the AD values never exceeded 0.50 mm. These results attest to the good accuracy of the DIC technique in being able to follow the global bond performance of different CFRP-to-timber bonded joints. Still, we should be bear in mind that in some specimens where a mechanical anchorage was used, the DIC technique failed to measure part of the area of interest that compromised the DIC measurements.

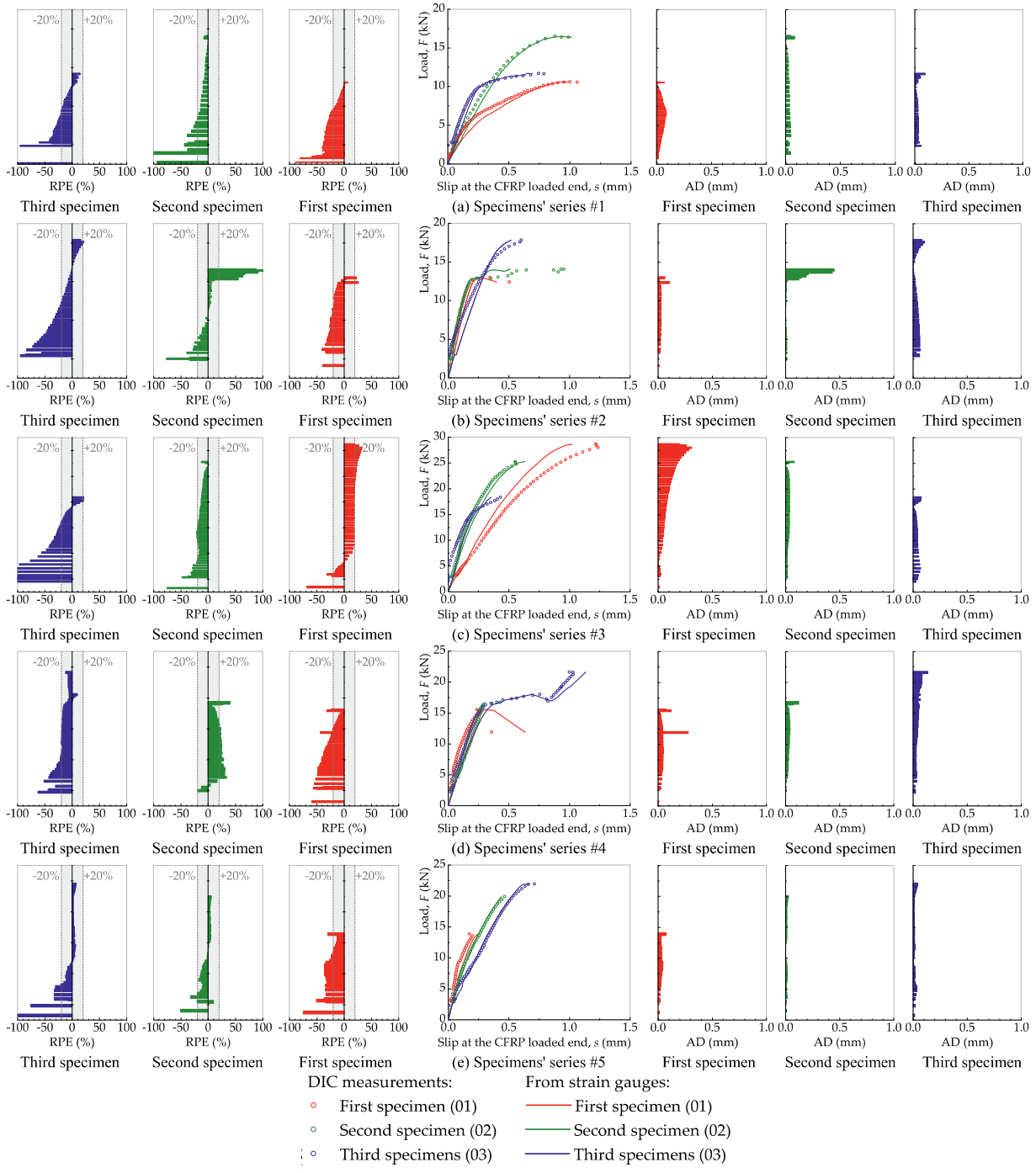

Fig. 6. Comparisons between the load-slip responses obtained from the DIC and from the strain gauge measurements.
Comparisons between the load-slip responses obtained from the DIC and from the strain gauge measurements.

3.2.3. Slip configurations

In the previous subsection, the global slips, *i.e.* the slips measured at the CFRP pulled end, determined from the DIC technique were compared with those determined from the strain gauge measurement through Eq. (6). In this subsection, the slips measured at different regions of the CFRP-to-timber bonded length are now shown. For the sake of simplicity of these analyses, the maximum of six slip configurations were considered. Therefore, six global slips, *i.e.* the slips at the CFRP pulled end, were considered (0.25, 0.50, 1.0, 1.5, 2.0 and 2.5 mm) and the corresponding slip configurations throughout the bonded length were obtained. Naturally, if those nominated global slips were not measured in the specimens, then the corresponding slip distributions cannot be shown.

Hence, Fig. 7 shows all the slip configurations obtained from all the tested specimens. Although the slip configurations obtained from the strain gauges are shown for all the specimens, to help the readability of this figure only the average results obtained from the DIC technique are shown. The average results obtained for each measurement technique (DIC and strain gauges) are compared through the RPE and AD values. The values of RPE and AD were based on both average slip configurations at the same distance from the pulled end, *i.e.* at the same points where the strain gauges were bonded onto the CFRP laminate.

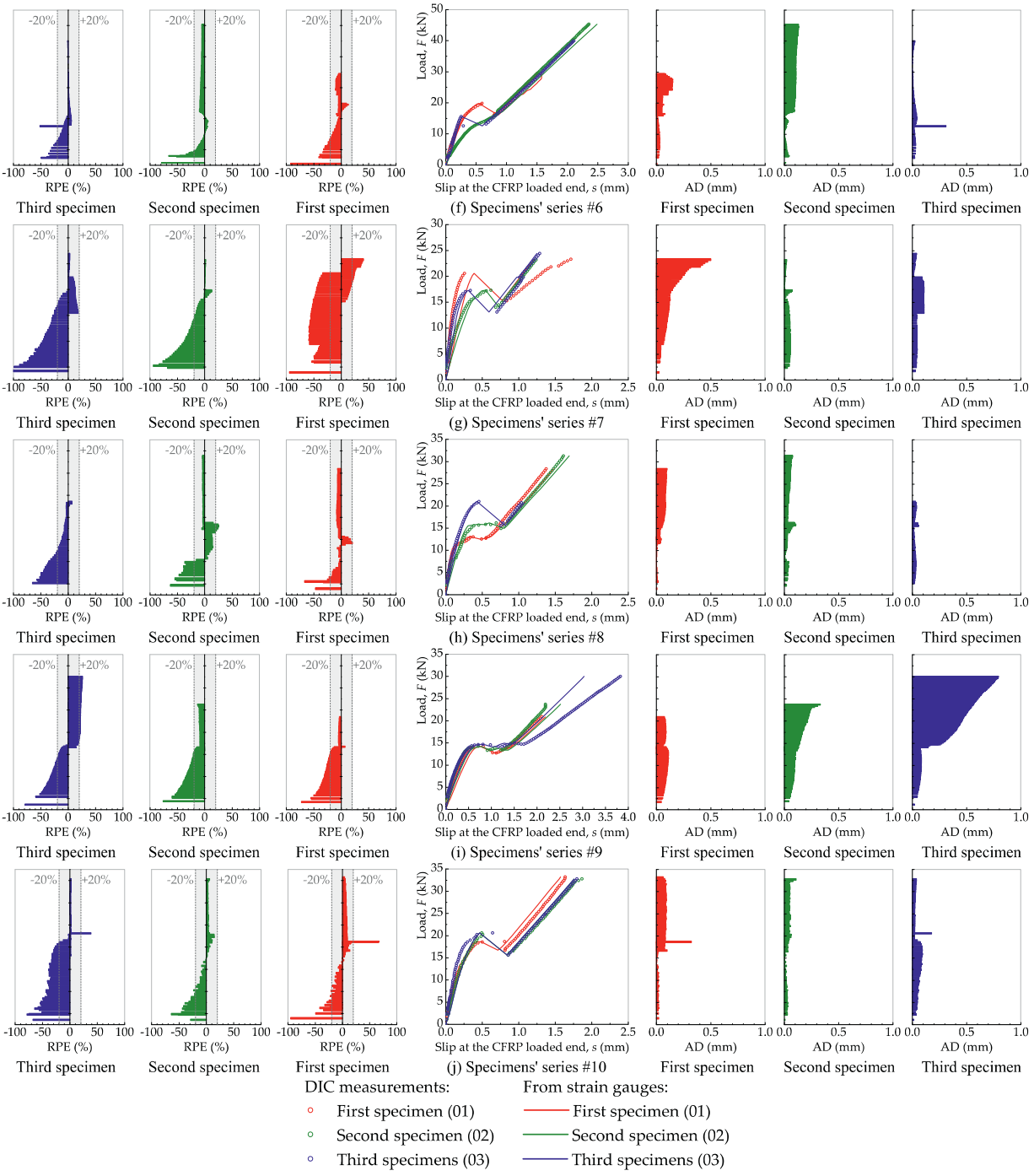

Fig. 6. Continued

In Fig. 7, it is possible to observe that the GIS1a and GIS1b specimens showed scatter results. The average configurations of these specimens showed a very good proximity between them when $s = 0.25$ mm. For the subsequent nominated global slips, the DIC technique underestimated the slips obtained from the strain gauges at all of the strain monitoring points. In fact, overall, the DIC technique underestimated the results obtained from the strain gauges, as can be seen from the calculated RPE values. Since the slips at the CFRP pulled end are the same in both measurement types and no slips are expected at the unpulled end, the RPE and the AD values are not reported in Fig. 7. Despite the considerable accuracy of the DIC measurements compared to those obtained from Eq. (6), it can be seen that the highest values of RPE are localized at the CFRP unpulled end region within which the slips have low magnitudes. On the other hand, the calculated AD values can be found somewhere in middle of the bonded length. Nevertheless, the calculated AD values never exceeded 0.50 mm.

In general, the DIC technique was able to track the typical nonlinear slip configurations as theorized by several authors in the literature [22, 53–60]. However, some fluctuations can be observed in the different slip configurations shown in Fig. 7, where the most visible ones can be seen in Figs. 7g and 7i, which correspond to the GIIS3 and GIIS5a specimens, respectively. Consequently, since the determination of the CFRP strains implies the differentiation with respect to the *y*-axis (*i.e.* the coordinate parallel to the bonded length) [12, 54, 56, 57, 61–64], it

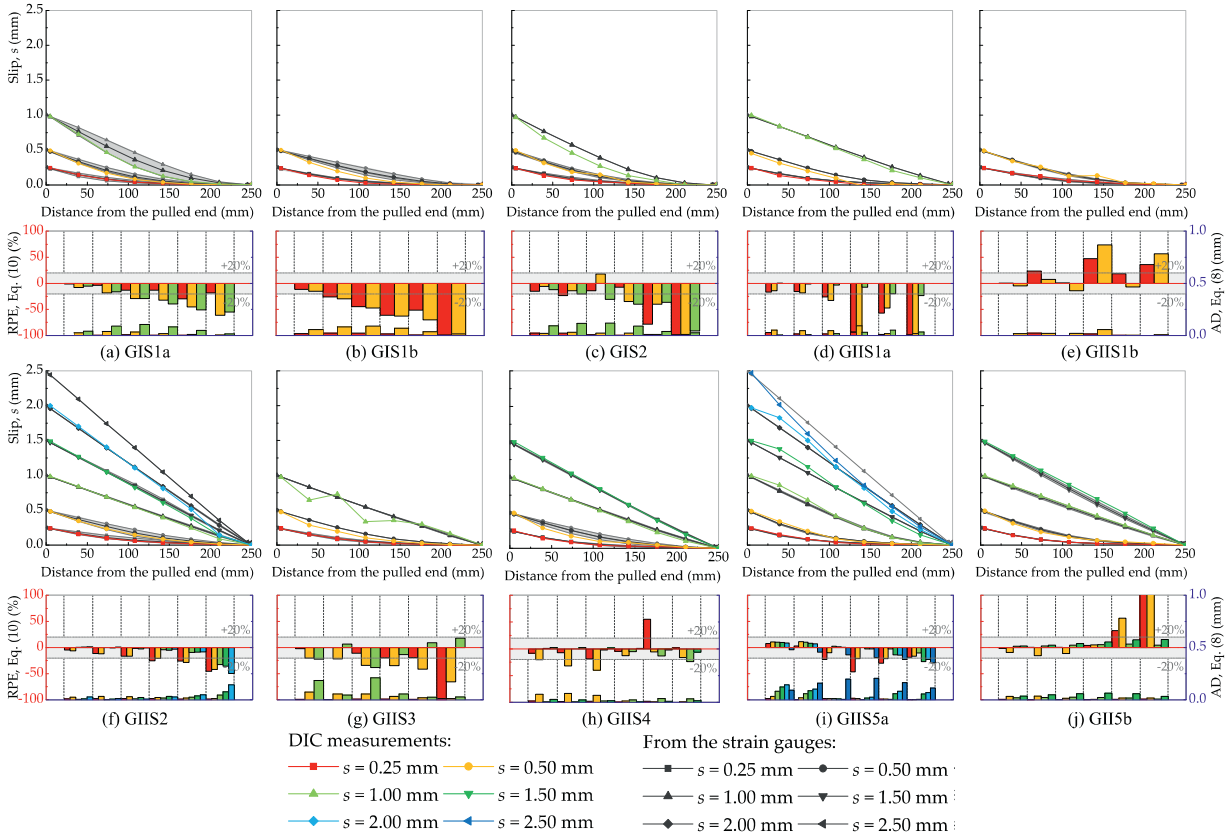

Fig. 7. Comparisons between the slip configurations obtained from the DIC and from the strain gauge measurements.

is expected that these fluctuations will be amplified. Thus, greater discrepancies would also be expected between the CFRP strains obtained from the DIC technique and from those obtained from the strain gauges. In addition, the determination of the bond stresses implies the calculation of the second derivative of the slips with respect to the *y*-axis, which makes it almost impossible to evaluate the bond assessment between an FRP composite and another parent material correctly. For these reasons, an approach based on two analytical and validated closed-solutions that bypasses those limitations is presented in Section 4.

4. Analytical-based analises of the results

In this section, the results obtained from the DIC measurements are compared with the experimental data as well with two different analytical solutions developed by the authors and implemented in references [47, 53]. Although bi-linear or tri-linear bond-slip relationships could adequately reproduce the local bond between a CFRP composite and a timber substrate, a well-known exponential bond-slip relationship [22] was selected. This option is justified by the versatility of that particular exponential bond-slip relationship when used to analytically describe the full debonding process between an FRP composite and another parent material substrate with [47] or without a mechanical anchorage [53].

4.1. Closed-form solutions

The bond behaviour between a CFRP composite and the substrate is very important in a structural reinforcement or in any other adhesively bonded structure. However, the premature debonding of the CFRP from the substrate is an issue that has been the subject of several studies, *e.g.* [47, 51, 57, 65–68]. To better understand this bond performance, Biscaia et al. [47, 53] have already proposed two distinct analytical solutions based on an exponential bond-slip relationship. Unlike Dai et al. [22] who have proposed a closed-form solution only for sufficient long bonded lengths, *i.e.* for bonded lengths greater than the effective bond length, the closed-form solution proposed by Biscaia et al. [47] estimates the bond performance of CFRP-to-parent material interfaces with no anchorages and independently of the bonded length of the joint. Additionally, the closed-form solution in reference [47] is also able to predict the snapback instability, whereas the closed-form solution in reference [22] cannot predict the complete load-slip response, mainly due to its simplicity, as will be shown later.

The other closed-form solution proposed by Biscaia et al. [47] can estimate the bond performance of perfectly anchored CFRP-to-parent material bonded joints. Like the model in reference [47], the model in reference [53] also estimates the full debonding process of adhesively bonded joints, but now with a mechanical anchorage. In both cases [47, 53] the models allow us to estimate the interfacial slips, the strains in the CFRP composite and the bond stress distributions at any point of the debonding process. Therefore, based on the DIC measurements, both analytical models were used to smooth the slip fluctuations already shown in the previous section and to enable us to evaluate the bond performance of the CFRP-to-timber joints with great precision that is as near to reality as possible. The results are always compared with those obtained from the strain gauge measurements.

Next, the two above-mentioned analytical models are presented briefly, where the following exponential bond-slip relationship proposed by Dai et al. [22] is used:

$$\tau(s) = 4\tau_{\max} \cdot \left(e^{-B \cdot s} - e^{-2B \cdot s}\right) \tag{12}$$

where $\tau_{\max}$ is the maximum bond stress developed within the adhesively bonded interface defined according to:

$$\tau_{\max} = \frac{B \cdot G_F}{2} \tag{13}$$

where B and G_F are, respectively, the stiffness index of the Mode II fracture energy of the adhesively bonded interface. Complementary to this local bond-slip model, the global load-slip response to a sufficient long bonded joint is approximated to:

$$F = F_{deb} \cdot \left(1 - e^{-B \cdot s}\right). \tag{14}$$

Despite being more complex, the proposal put forward by Biscaia et al. [53] for FRP-to-parent material bonded joints free of any mechanical anchorages leads to the following slip equation along the bonded length:

$$s(y) = \frac{1}{B} \cdot \ln\left[\frac{e^{(D\cdot y + C_2)\cdot\left(B\cdot\sqrt{1-\left(1-e^{-B\cdot s_0}\right)^2}\right)} + 2 + 2\cdot\sqrt{1-\left(1-e^{-B\cdot s_0}\right)^2}}{2\cdot\sqrt{1-\left(1-e^{-B\cdot s_0}\right)^2} + 2\cdot\left[1-\left(1-e^{-B\cdot s_0}\right)^2\right]}\right] \tag{15}$$

where:

$$C_2 = \frac{\ln\left[e^{B\cdot s_0}\cdot\left(2\cdot\sqrt{1-\left(1-e^{-B\cdot s_0}\right)^2} + 2\cdot\left(1-\left(1-e^{-B\cdot s_0}\right)^2\right)\right) - 2 - 2\cdot\sqrt{1-\left(1-e^{-B\cdot s_0}\right)^2}\right]}{B\cdot\sqrt{1-\left(1-e^{-B\cdot s_0}\right)^2}} \tag{16}$$

$$D = \sqrt{\frac{2G_F}{E_f\cdot t_f}\cdot(1+\beta)^2} \tag{17}$$

and s_0 is the slip at the FRP free end which is imputed into the model; and y corresponds to the coordinate parallel to the bonded length which, in this model, has its origin at the FRP unpulled end. Thus, taking into account Eq. (15), the global load-slip response (at $y = L_b$) can be mathematically reproduced according to [53]:

$$F = E_f t_f b_f \cdot D \cdot \sqrt{\left(1 - \frac{2\cdot\sqrt{1-\left(1-e^{-B\cdot s_0}\right)^2} + 2\cdot\left[1-\left(1-e^{-B\cdot s_0}\right)^2\right]}{e^{(D\cdot L_b + C_2)\cdot\left(B\cdot\sqrt{1-\left(1-e^{-B\cdot s_0}\right)^2}\right)} + 2 + 2\cdot\sqrt{1-\left(1-e^{-B\cdot s_0}\right)^2}}\right)^2 - \left(1-e^{-B\cdot s_0}\right)^2} \tag{18}$$

where L_b correspond to the bonded length of the adhesively bonded joint. The estimation of the bond stresses at any point of the adhesively bonded joint are defined by:

$$\tau(y) = 2B\cdot G_F \cdot \left[\frac{2\cdot\sqrt{1-\left(1-e^{-B\cdot s_0}\right)^2} + 2\cdot\left[1-\left(1-e^{-B\cdot s_0}\right)^2\right]}{e^{(D\cdot y + C_2)\cdot\left(B\cdot\sqrt{1-\left(1-e^{-B\cdot s_0}\right)^2}\right)} + 2 + 2\cdot\sqrt{1-\left(1-e^{-B\cdot s_0}\right)^2}} - \left(\frac{2\cdot\sqrt{1-\left(1-e^{-B\cdot s_0}\right)^2} + 2\cdot\left[1-\left(1-e^{-B\cdot s_0}\right)^2\right]}{e^{(D\cdot y + C_2)\cdot\left(B\cdot\sqrt{1-\left(1-e^{-B\cdot s_0}\right)^2}\right)} + 2 + 2\cdot\sqrt{1-\left(1-e^{-B\cdot s_0}\right)^2}}\right)^2\right]. \tag{19}$$

In anchored FRP-to-parent material bonded joints, the slip distributions along the bonded length can be predicted by using the following equation [47]:

$$s(y) = \frac{1}{B}\cdot\ln\left[\frac{\sinh\left(\left(D\cdot y + \frac{\operatorname{arcsinh}\left(\frac{\varepsilon_0}{D}\right)}{B\cdot\sqrt{1+\left(\frac{\varepsilon_0}{D}\right)^2}} + B\cdot\sqrt{1+\left(\frac{\varepsilon_0}{D}\right)^2}\right) + \frac{D}{\varepsilon_0}\right)}{\frac{\varepsilon_0}{D} + \frac{D}{\varepsilon_0}}\right] \tag{20}$$

where ε_0 is the strain in the FRP composite at the FRP anchored end, which should be monotonically increased in the model to obtain the full debonding process of the anchored FRP-to-parent material interface. Along with Eq. (20), the prediction of the global load-slip response of anchored bonded joints, can be carried out using the following equation:

$$F = E_f\cdot t_f\cdot b_f\cdot\sqrt{D^2\cdot\left[1 - \frac{\frac{\varepsilon_0}{D} + \frac{D}{\varepsilon_0}}{\sinh\left(\left(D\cdot L_b + \frac{\operatorname{arcsinh}\left(\frac{\varepsilon_0}{D}\right)}{B\cdot\sqrt{\left(\frac{\varepsilon_0}{D}\right)^2+1}}\right)\cdot B\cdot\sqrt{\left(\frac{\varepsilon_0}{D}\right)^2+1}\right) + \frac{D}{\varepsilon_0}}\right]^2 + {\varepsilon_0}^2} \tag{21}$$

whereas the interfacial bond transfer between materials is defined according to [47]:

$$\tau(y) = 2B\cdot G_F\cdot\left[\frac{\frac{\varepsilon_0}{D} + \frac{D}{\varepsilon_0}}{\sinh\left(\left(D\cdot y + \frac{\operatorname{arcsinh}\left(\frac{\varepsilon_0}{D}\right)}{B\cdot\sqrt{\left(\frac{\varepsilon_0}{D}\right)^2+1}}\right)\cdot B\cdot\sqrt{\left(\frac{\varepsilon_0}{D}\right)^2+1}\right) + \frac{D}{\varepsilon_0}} - \left(\frac{\frac{\varepsilon_0}{D} + \frac{D}{\varepsilon_0}}{\sinh\left(\left(D\cdot y + \frac{\operatorname{arcsinh}\left(\frac{\varepsilon_0}{D}\right)}{B\cdot\sqrt{\left(\frac{\varepsilon_0}{D}\right)^2+1}}\right)\cdot B\cdot\sqrt{\left(\frac{\varepsilon_0}{D}\right)^2+1}\right) + \frac{D}{\varepsilon_0}}\right)^2\right]. \tag{22}$$

In both closed-form solutions, the definition of the stiffness index B and the Mode II fracture energy (G_F) should be known first. Consequently, the fitting process to obtain the bond-slip relationship of the joint is highly relevant for its precise definition, as will be discussed in the next subsection. After that, the full debonding processes of the several CFRP-to-timber joints herein considered can be finally estimated and described without amplifying errors introduced by the DIC measurements, as already mentioned.

4.2. Fitting process for the definition of the bond-slip relationship

Like other adhesively bonded structures, *e.g.* [18, 19], a fitting procedure to define the bond-slip relationship could be an effective method

for the determination of the local bond-slip relationship of CFRP-to-timber material joints. Nevertheless, to make comparisons between the DIC results and those obtained from the use of strain gauges, it should be briefly explained how the bond stresses are calculated from the strain gauge measurement. Thus, the bond stresses can be determined from the following equilibrium condition of a finite length *dy* [42, 47, 53]:

$$\tau = t_f \cdot \frac{d\sigma_f}{dy} \tag{23}$$

where σ_f is the axial stress in the FRP composite. Assuming a linear constitutive behaviour of the FRP composite, Eq. (23) can be numerically solved according to:

$$\tau\left(y_{i+1/2}\right) = E_f t_f \cdot \frac{\varepsilon_{f,i+1} - \varepsilon_{f,i}}{y_{i+1} - y_i}. \tag{24}$$

To correctly define the local bond-slip relationship, the bond stresses and the slips still need to be coupled at the same exact points $y_{i+1/2}$, which is ensured if the slips at that same point are determined according to:

$$s\left(y_{i+1/2}\right) = \frac{s\left(y_{i+1}\right) + s\left(y_i\right)}{2} \tag{25}$$

where the slips measured at points y_{i+1} and y_i are determined from Eq. (6).

For the fitting process to determine the theoretical bond-slip relationship defined in Eq. (12), a minimization process, where the lowest square minimization process between the theoretical bond stress (τ_i) defined in Eq. (12) and the experimental bond stress determined from Eq. (24), is established. However, as already mentioned, the DIC measurements *per se*, lead to amplified bond stresses and consequently the exclusive use of their results within the minimization process may not be sufficient to correctly estimate the global load-slip response of the bonded joint. As already shown, the DIC technique was able to accurately describe the debonding process up to the debonding load, and for this same reason, it is important to add into this minimization process a second condition where the square minimization process between the theoretical loads transmitted to the CFRP laminate (F) and the experimental ones (F_{exp}) should be considered. This way, it ensures that the local bond-slip relationship will accurately reproduce both local and global bond behaviours. This minimization procedure can be mathematically defined according to:

$$\xi = \min_{B} \begin{cases} \sum_{t=1}^{n} \left(\tau_t - \tau_{\text{exp},t}\right)^2 \\ \sum_{t=1}^{n} \left(F_t - F_{\text{exp},t}\right)^2 \end{cases} \tag{26}$$

where τ_t and $\tau_{\text{exp},t}$ are the bond stresses obtained from the theoretical Eq. (12) and from the bond stresses obtained from the DIC measurements; and F_t and $F_{\text{exp},t}$ are the theoretical loads transmitted to the CFRP laminate (determined from Eq. (14) or from Eq. (18) in the case of unanchored CFRP-to-timber joints and from Eq. (21) if the CFRP laminate is anchored to the timber substrate), and the experimental loads at different instants t of the test duration. In addition to this minimization process, the following constraint was also added:

$$G_F = \frac{{F_{deb}}^2}{(1+\beta) \cdot E_f \cdot t_f \cdot {b_f}^2} \tag{27}$$

where G_F is the fracture energy.

Hence, the use of this minimization process led to the theoretical bond-slip relationships shown in Fig. 8. To facilitate the readability of this figure, only the average local bond-slip relationships obtained from the three tested specimens of each series are shown. In addition, Table 3 summarizes the values of the parameters found from the minimization process in (26) carried out to define each theoretical bond-slip relationship. It should be mentioned here that to obtain the local bond-slip relationships of each tested specimen the values measured at 39.3 mm, 73.6 mm and 107.9 mm from the CFRP pulled end were considered.

Table 3
Summary of the determined parameters of the local bond-slip relationhsip.

ID	Fracture energy, G_F (N/mm)	IAE (%)	Stiffness index, B (mm^{-1})				Maximum bond stress, τ_{max} (MPa)			
			From the strain gauges	From the DIC measurements	RPE (%)	AD (mm^{-1})	From the strain gauges	From the DIC measurements	RPE (%)	AD (MPa)
GIS1a	2.848	18.1	4.88	4.16	−14.8	0.72	6.95	7.03	1.2	0.08
GIS1b	1.771	25.7	8.31	8.00	−3.7	0.31	7.36	9.54	29.6	2.18
GIS2	6.708	69.5	2.93	5.55	89.4	2.62	9.44	14.81	56.9	5.37
GIIS1a	3.157	74.6	3.50	7.35	110.0	3.85	5.49	11.30	105.8	5.81
GIIS1b	3.994	73.7	3.39	6.81	100.9	3.42	6.23	10.89	74.8	4.66
GIIS2	2.591	15.4	5.14	5.36	4.3	0.22	6.66	8.20	23.1	1.54
GIIS3	3.495	60.4	5.11	9.37	83.4	4.26	8.93	17.88	100.2	8.95
GIIS4	3.170	50.8	5.78	9.25	60.0	3.47	9.16	12.65	38.1	3.49
GIIS5a	4.118	25.4	3.56	4.52	27.0	0.96	7.33	9.90	35.1	2.57
GIIS5b	3.958	10.5	5.78	5.37	−7.1	0.41	11.44	11.84	3.5	0.40

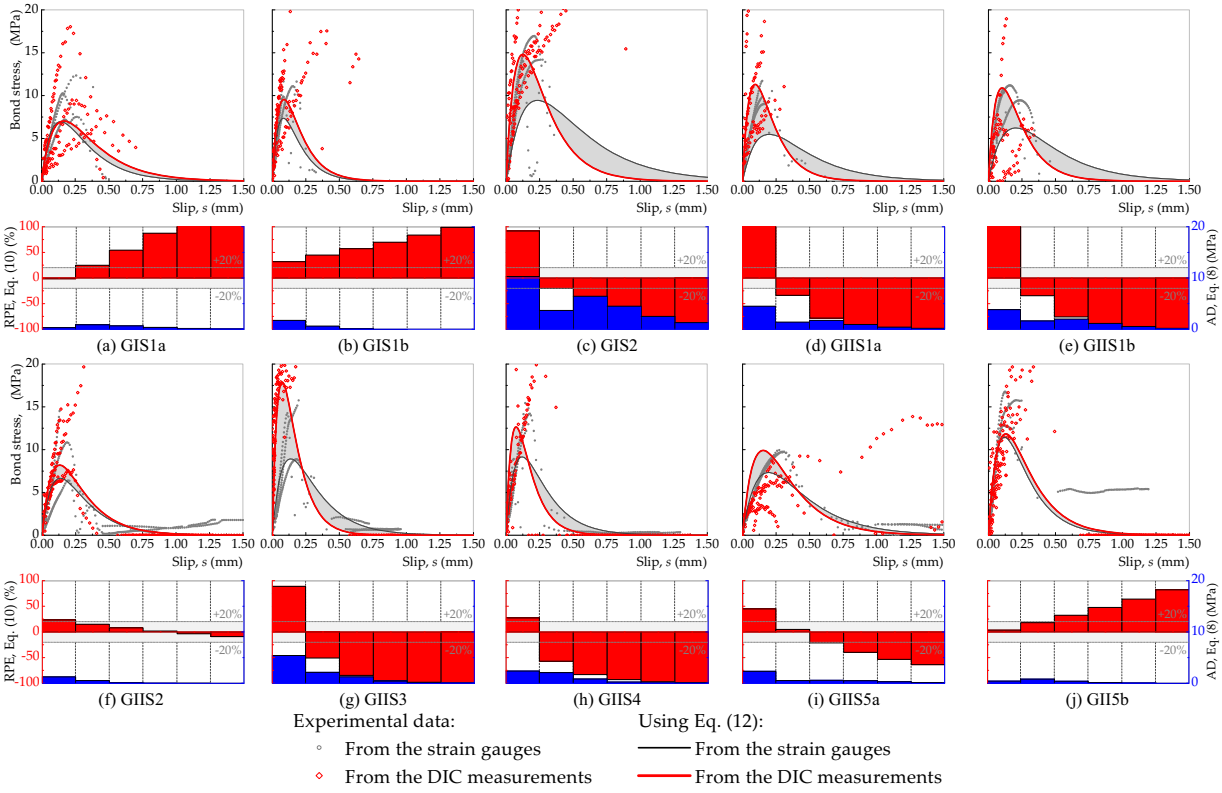

Fig. 8. Comparison between the theoretical bond-slip relationships obtained from the DIC measurements and those obtained from the strain gauge measurements.

Therefore, no perpendicular stresses to the bonded surface were expected to occur and affect the results as described in the literature, *e.g.* [20, 69–71].

Based on these results, it can be stated that in some specimen series large differences were observed between the use of the DIC technique with the strain gauges and no consistent observation could be drawn for all the tested specimens. For instance, in series GIS2, GIIS1a, GIIS1b or GIIS3, the value of IAE ranged between 60% and 75%, which reveals some lack of accuracy between measurement methods. Particularly in specimen series GIIS1a and GIIS3, the use of the DIC measurements led to maximum bond stresses that exceeded 100% of that obtained from the use of the strain gauges. Nevertheless, in specimen series GIS1a, GIIS2 and GIIS5b, the use of both methods replicated almost the same theoretical bond-slip relationship. Particularly in GIS1a and GIIS5b, the relative difference of the maximum bond stresses obtained from both measurements methods is almost negligible (1.2% and 3.5%, respectively).

Although not within the scope of this work, a note about the implications of the differences already identified in the definition of the effective bond length (L_{eff}) should be given. By definition, the effective bond length of a bonded joint is the length beyond which the load transmitted to the CFRP composite cannot continue increasing any longer. The definition of this parameter is important as is stated by several authors [57, 72, 73] that have derived different equations to define it. It seems consensual that the increase in the stiffness $E_f t_f$ increases the effective bond length, whilst fracture energy decreases it. Considering the same specimen series, these parameters are the same and they should not influence the effective bond length. However, the softening stage of the bond-slip relationship, *i.e.* the stage after the maximum bond stress is reached, may introduce some differences in the calculation of the effective bond length. For instance, if the softening stage has a more of an abrupt decay rather than a smooth decay, then the effective bond length will decrease [74, 75] due to a lower ultimate slip. So, as could be seen from the bond-slip relationships in Figs. 8c-e or 8 g-h, the DIC measurements will lead to a lower effective bond length than that given by the strain gauge measurements. As a consequence, the use of the DIC measurements may lead to unsafe situations due to the obvious reductions of the bonded length causing a direct reduction in the strength of the joint. Therefore, and erring on the side of caution, the use of the 2D DIC technique to evaluate the bond assessment should be seen as a complementary technique to other well-established measurement methods and not as the main or only method of measuring. Apart from this, and as will be seen in the subsequent subsections, the use of all these local bond-slip relationships did not produce meaningful differences from the debonding process of the CFRP-to-timber joints described with the help of the strain gauges.

4.3. Predicted debonding processes of the specimens

4.3.1. Global load-slip curves

The global load-slip curves of all the specimen series are shown in Fig. 9. As already explained in subSection 3.2.2., the global load-slip curves are quite different between the groups, *i.e.* depending on whether a mechanical anchorage is used or not. In Figs. 9a-c, the use of Eqs. (15) and (18) is compared to the experimental results, in particular to the average results, which are identified as a black line in the centre of the grey region that covers the experimental data. From these first three figures, it can be seen that the debonding load is accurately estimated as would be expected due to the introduction of the constraint (27) in the minimization process carried out for the determination of the bond-slip relationship in (26). The initial branch of the predicted load-slip curves is quite similar to the one obtained from use of strain gauges. Since the loads were monotonically applied to the CFRP laminates, when the strength of the adhesively bonded joint was reached no further data was collected from the strain gauges and, unlike the predicted load-slip curve, no snap-back instability could be identified.

Of these three specimens, the GIS2 specimens had the highest calculated values of RPE when the load transmitted to the CFRP laminate had low magnitudes. As the loads increased, these values tended to decrease

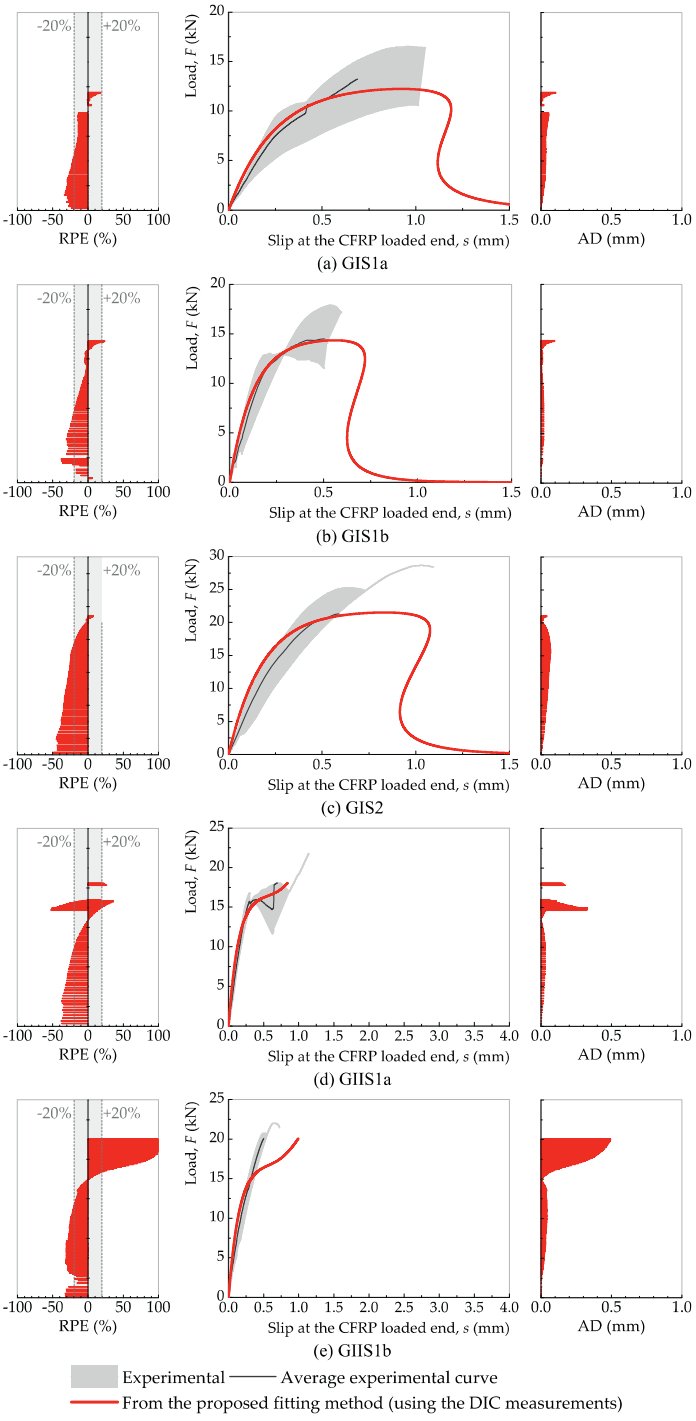

Fig. 9. Comparison between the global bond-slip curves obtained from the DIC measurements (using a closed-form solution) and the strain gauge measurements.

Comparison between the global bond-slip curves obtained from the DIC measurements (using a closed-form solution) and the strain gauge measurements.

and at the debonding low, the RPE value is almost negligible. Moreover, the values of AD were quite low in the first three series, which also confirms the high level of accuracy of the combination between the closed-form solution and the DIC measurements with the data obtained from the strain gauges.

In the second group of specimens, the load-slip curves predicted by the closed-form solution (see Eqs. (20) and (21)), tracked the average curve obtained from the use of strain gauges very closely. Nevertheless, a couple of issues should be pointed out. The first one corresponds to the initial stage of debonding at the debonding load. Within this part of both load-slip curves, it can be observed that the closed-form solution provided a smooth transition from the debonding load to the next stage, whilst a rather irregular transition is observed in the results obtained from the gauge measurement. Consequently, and within this part of all load-slip curves, the highest values of RPE and AD were calculated here. Although in none of the present cases the value of AD exceeded 0.60 mm, in some (see Figs. 9e, 9g-h) the values of RPE exceeded 100% at this load magnitude (*i.e.* at the debonding load). The other issue occurred only in specimen series GIIS1b and GIIS3, where the theoretical load-slip curve clearly predicted the initiation of debonding at a lower load magnitude than that which was determined from the measurements made with the strain gauges. Consequently, the AD value in the GIIS1b series almost reached 0.50 mm, whereas in the GIIS3 series the maximum AD value did not exceeded 0.45 mm.

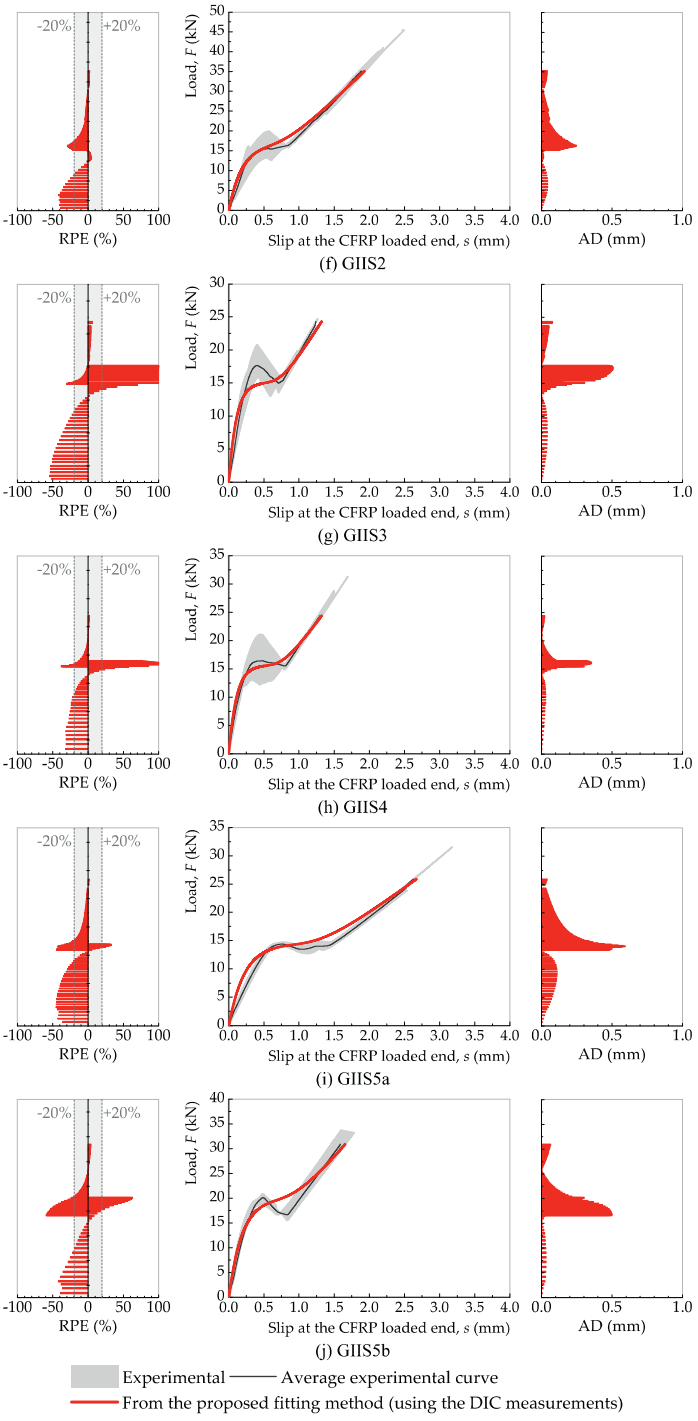

Fig. 9. Continued

Generally, when the load transmitted to the CFRP laminate has a low magnitude, the RPE values are all negative, which means that, for a fixed slip, the closed-form solution is overestimating the load when compared with the data collected from the strain gauges. However, as the load increases the calculated RPE tends to a marginal value. With the exceptions already identified above, the post-debonding stages of the theoretical load-slip curves indicate good agreement between measurement methods, with negligible RPE values and low AD values.

4.3.2. Slip configurations

Fig. 10 shows the slip configurations obtained from the closed-form solution in Eqs. (15) and (20) in which the theoretical bond-slip relationships were obtained from the DIC measurements. For the sake of simplicity, only the average values obtained from both measuring methods are presented. Furthermore, the slip configurations shown in Fig. 10 correspond to the same previously nominated slips at the CFRP loaded end, *i.e.* at s = 0.25, 0.50, 1.0, 1.5, 2.0 and 2.5 mm. In some specimen series only part of these fixed slips were reached due to the rupture of the specimens and, therefore, only the data corresponding to the fixed slips obtained in the experiments are presented from hereafter.

At the lowest slip magnitude, the slips measured by both methods are quite similar as proved by the residual values of AD. The highest RPE values can be observed in all the specimens when s = 0.25 mm. However, this can be easily explained by the very small values associated to

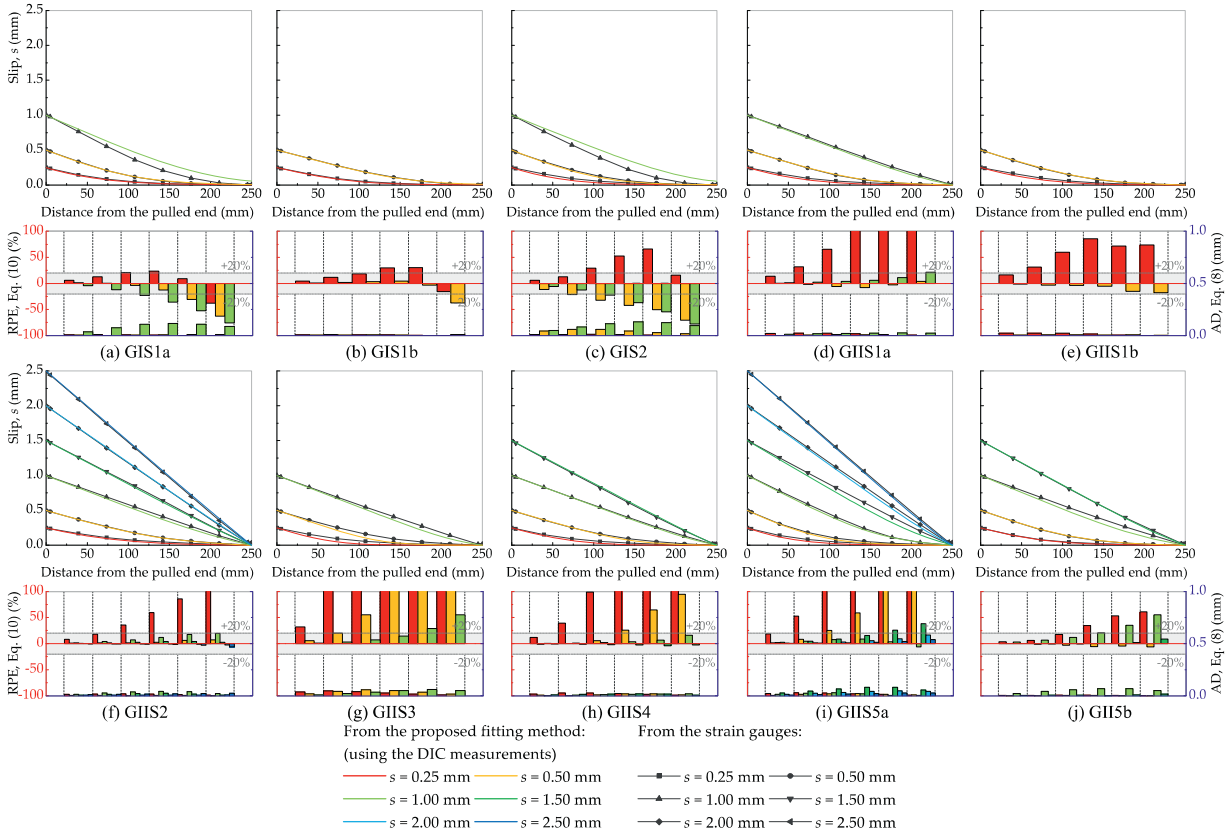

Fig. 10. Comparison between the slip configurations obtained from the DIC measurements (using a closed-form solution) and the strain gauge measurements.

this first slip configuration that amplifies the calculated values of RPE. In the subsequent nominated slips, remarkable parity continues to be observed between the closed-form solutions and the data collected from the strain gauges. Nevertheless, and unlike the direct measurements carried out from the DIC technique, where the slips were underestimated when compared with the strain gauges measurement of specimen series GIS1a and GIS2 (see Figs. 7a and 7c, respectively), now, the closed-form solution is overestimating the interfacial slips at different points of the bonded length (see Figs. 10a and 10c). Compared with all the slip configurations shown in Fig. 7, the fluctuations were all eliminated, as would be expected, with the use of the closed-form solutions.

4.3.3. CFRP strains throughout the bonded length

The strains developed in the CFRP laminate are presented in Fig. 11 for all specimen series at the six nominated slips defined previously. Once again, to help make the data in Fig. 11 more readable and after adopting a linear constitutive behaviour of the CFRP laminates, the strains obtained from the closed-form solutions in (18) and (21) are compared to the average results obtained from the strain gauge measurements.

The first point that can be observed from Figs. 11a and 11b is the decrease in the maximum CFRP strain with the increase of the CFRP thickness. Nevertheless, at $s = 1.0$ mm, some differences between the two measurements can be seen in the GIS1a specimens. Based on the DIC measurements, the closed-form solution in (18) underestimated the CFRP strains obtained from the strain gauges at $s = 1.0$ mm but showed a very good agreement in the other two lower fixed slips, whether in the GIS1a or GIS1b specimens. Like the GIS1a specimens, the results obtained from the DIC measurements agreed very closely with those obtained from the strain gauge measurements in the GIS2 specimens at the first two nominated slips (see Fig. 11c), but showed some differences when $s = 1.0$ mm. In fact, this is clearly shown by the RPE and AD values where the former exceeds 100% at the vicinities of the CFRP unpulled end, whereas the latter led to an absolute CFRP strain difference of approximately 0.12% at the point closest to the CFRP loaded end.

The development of the CFRP strains along the bonded length at the lowest nominated slips are all quite similar in all the specimens, whether they have a mechanical anchorage at the CFRP unpulled end or not. With the exception of the GIIS1b specimens, where the closed-form solution in (21) overestimated the CFRP strains measured by the strain gauges, these were very well tracked by those obtained from Eq. (21). In these nominated slips, the CFRP strains at the CFRP pulled end registered the highest values. However, the CFRP strains nonlinearly decrease towards the CFRP unpulled end, in which a zero value is reached. However, the shape of this strain distribution changes when the mechanical anchorage begins to influence the performance of the CFRP-to-timber joint. Thus, it is possible to see that the CFRP strains at the CFRP unpulled end increases, which means that the anchorage is now responsible for the laminate not completely detaching from the timber prism. During this process, the CFRP laminate debonds from the timber substrate and within the corresponding unbonded length, a plateau can be seen in the distribution of the CFRP strains along the initial bonded length. This configuration of the CFRP strains is clearly seen with both the strain gauge measurements and, as would be expected, the closed-form in (21).

However, it should be pointed out that despite incorporating a mechanical anchorage in the GIIS1a and GIIS1b specimens (with 2 and 3 CFRP spike anchors, respectively), it was only possible to increase the debonding load in one specimen (SGIIS1a-03), and even then only marginally. As a consequence, the above-mentioned CFRP strain distributions observed from the other anchored CFRP-to-timber joints could not be seen in these particular GIIS1a and GIIS1b specimens, which means that these anchors failed to delay or even prevent the premature debonding of the CFRP from the timber prism.

Furthermore, three main points can be raised from these analyses. One is the fact that by using the DIC measurements in order to use the

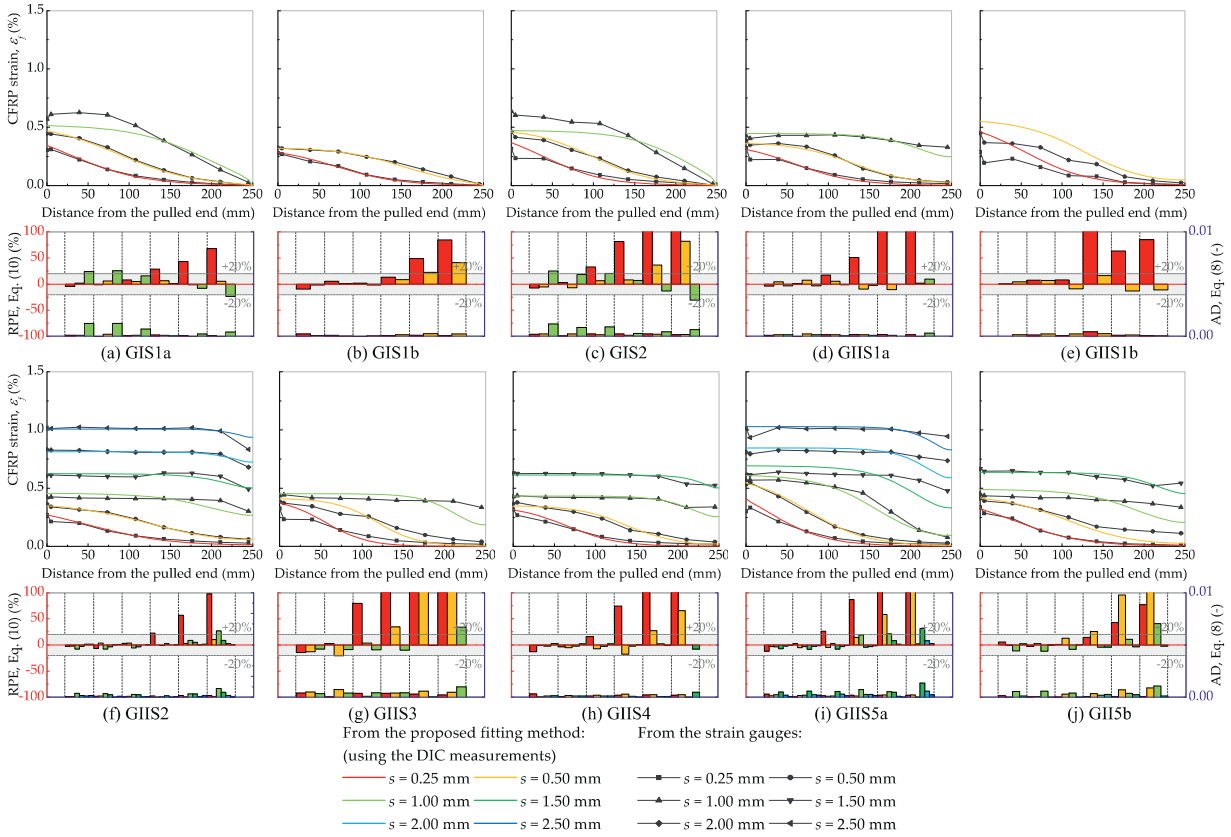

Fig. 11. Comparison between the CFRP strains along the bonded length obtained from the DIC measurements (using a closed-form solution) and the strain gauge measurements.

closed-form solution in (21), the CFRP strain configurations show none of undesirable fluctuations that are known to occur when the strains are based directly on the DIC measurements [18, 23, 41, 42]. The second is the good agreement that the results obtained from the closed-form solution in Eq. (21) showed when compared with the strain gauge measurements. The third and final point is the lack of data obtained from the DIC measurements in several specimens after the debonding load as mentioned above. Despite this, and with the use of Eq. (21) along with the methodology herein followed, it was still possible to perform the debonding analysis of the anchored CFRP-to-timber joint without compromising the subsequent interpretations of the results. In these circumstances, the calculated AD values of the highest nominated slips never exceeded 0.15%.

4.3.4. Interfacial transfer of bond stresses

The analysis of the bond transfer between the CFRP laminate and the timber substrate deserves particular attention since it requires de calculation of the second derivative with respect to the *y*-axis (parallel to the bonded length), which significantly amplifies the fluctuations of the slips obtained from DIC measurements [18, 41, 42]. In other words, the identification of the interfacial bond stress transfer will be hard to carry out if equation [18, 61, 68, 76–78]

$$\tau = E_f \cdot t_f \frac{d^2 s}{dy^2} \tag{28}$$

is used rather than the use of Eq. (19) and (22). Nevertheless, the use of strain gauges implies the use of the first derivative with respect to *y* as defined in Eq. (24) and, therefore, some fluctuations can be seen from the bond stresses obtained with the strain gauges. Conversely, the closed-form solutions clearly show how the bond stresses are transferred along the bonded length of the CFRP-to-timber joints at the six predefined slips. Nevertheless, when both methods are compared in the RPE and AD values, it can be seen that the former greatly exceeded 100% on several occasions, whilst the latter exceeded, or almost reached, 10.0 MPa on several occasions (see Fig. 12).

The interfacial bond stress transfer within the bonded length of the CFRP-to-timber joint has different characteristics depending on whether a mechanical anchorage is used or not. For instance, in the specimens in the first group (GIS1a, GIS1b and GIS2), the bond stresses show that as the slips increase the maximum bond stresses in each specimen series tend to migrate from the CFRP pulled end towards the unpulled and CFRP free end. This same characteristic can also be seen in the second group of specimens with a mechanical anchorage at the first two lowest nominated slips (*i.e.s* = 0.25 and 0.50 mm). However, and even at the fixed slip of 0.50 mm, the main difference between these two groups can be seen at the CFRP unpulled end. For instance, in Fig. 11b, both measurement methods show that the bond stresses at the CFRP unpulled end of the GIS1b specimens do not have a zero value, whereas in, *e.g.*, the GIIS2 specimens, the DIC measurements show a region close to the mechanical anchorage where the bond stresses tend to a zero value. In fact, for the other highest nominated slips, the bond stresses tend to concentrate close to the mechanical anchorage within a limited length, which is also confirmed by the calculations made using Eq. (24). On the other hand, in the opposite region, *i.e.* close to the CFRP pulled end, residual bond stresses were determined by both measuring methods.

Conclusions

The present work analysed the use of 2D DIC technique to evaluate two different debonding processes for anchored and unanchored CFRP laminates attached to a timber prism. To that end, two closed-form solutions were used in which a theoretical and exponential bond-slip relationship was derived from the DIC measurements. The accuracy of the DIC measurements was analysed by comparing the results with ho-

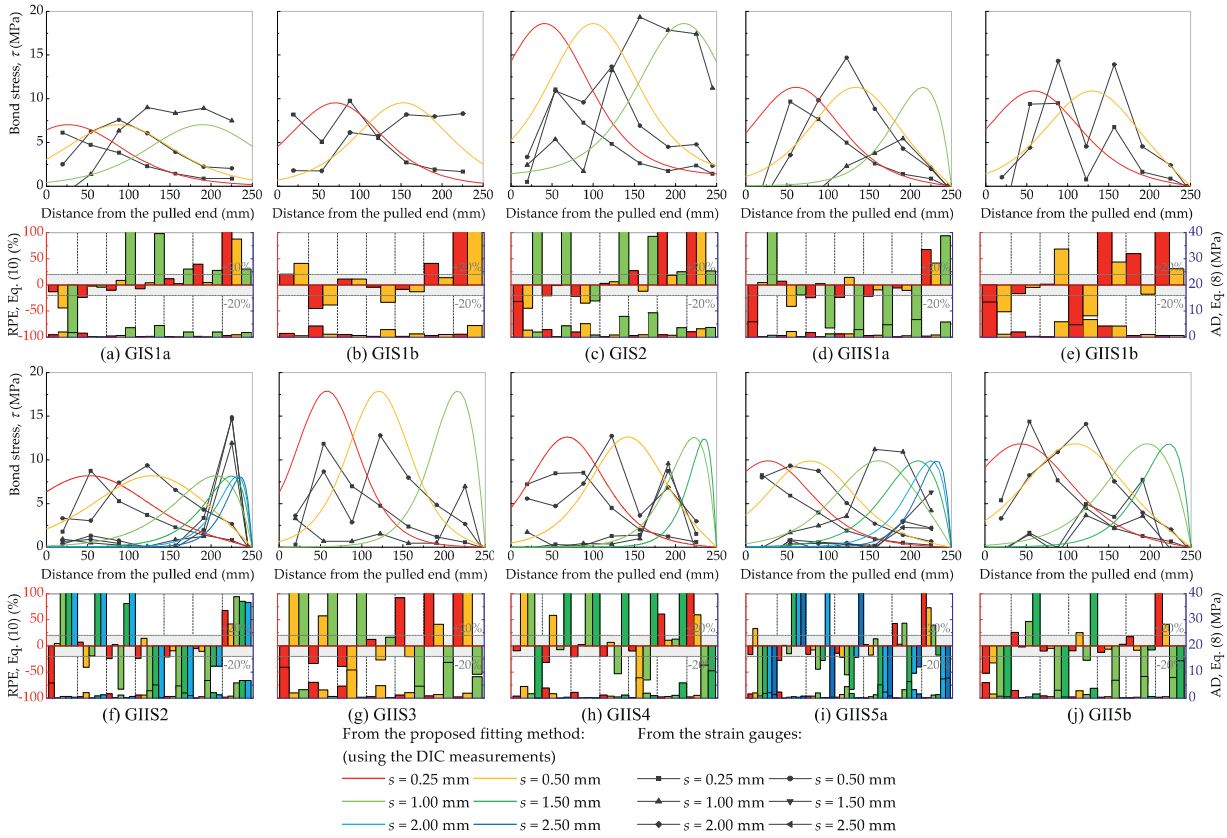

Fig. 12. Comparison between the interfacial bond stress transfer obtained from the DIC measurements (using a closed-form solution) and the strain gauge measurements.

mologous ones obtained from a well-established measuring method, *i.e.* through the use of electric strain gauges. Based on the results achieved in this work, the following main conclusions can be drawn:

- considering both group specimens, *i.e.* with and without the mechanical anchorage, the GIIS2 and GIIS51a specimen series reached the highest ultimate loads, *i.e.* the specimens where two superposed L-shaped metallic profiles were used and where the CFRP unpulled end was embedded into the timber prism, respectively;
- the 2D DIC technique was able to match the measurements carried out from the strain gauges during the test period. However, as the debonding load was reached in the second specimen group, the DIC technique failed to record several facets of consecutive photos. This flaw was attributed to the fact that the intervals between photos was 5 s and when the CFRP debonded from the timber prism led to a fast slip increase of approximately 0.5 mm, it somehow made impossible for the DIC technique to capture several facets and measure their displacements within the area of interest;
- bearing in mind the previous conclusion, the new proposed methodology, *i.e.* the use of the closed-form solutions based on the DIC measurements, allowed us to bypass the flaw obtained from the DIC technique, since it requires only the definition of the bond-slip relationship, which was completely obtained from the DIC measurements up until the debonding load. Still, it was also concluded that in the determination of the bond-slip relationships of all the specimen series, the global load-slip response of the CFRP-to-timber joints should be also taken into account;
- although the DIC and the strain gauge measurements have had good parity, the slips obtained from the former led to some fluctuations that were amplified when the CFRP strains were calculated. Consequently, the values of the bond stresses tended to be overestimated when compared with those obtained from the strain gauges. Moreover, and despite not being reported here, it would have led to even higher fluctuations of the bond stress transfer along the bonded length, which would have made the interpretation of the test results difficult;
- the determination of the local bond-slip relationships from the DIC measurements showed some differences from those obtained with the strain gauges. Thus, and in some specimen series, the use of the DIC technique led to local bond-slip relationships with higher maximum bond stresses (AD < 10.0 MPa) and with less smoother decays after that peak bond stress. GIIS1a and GIIS1b registered the highest IAE values (~75%). However, these differences did not significantly affect the global load-slip responses of the CFRP-to-timber joints;
- the use of the proposed methodology allowed us to conclude that the exponential bond-slip relationship is quite versatile, as was shown by the proximity of the closed-form solutions to the strain gauge measurements in the slip, CFRP strain and bond stress distributions of different types of CFRP-to-timber bonded joints.

It should be also noted that the results herein reported were obtained from an inexpensive monitoring solution, in which the 2D DIC technique and an ordinary digital camera were used. No comparisons were made with the Stereo DIC technique, and the use of better digital cameras would improve the research into the evaluation of the debonding process of different CFRP-to-timber joints. The authors therefore recommend some caution when the evaluation of CFRP-to-timber bonded joints is carried out for the first time using these contactless techniques, and that the techniques be used in tandem with other well-established monitoring techniques.

Declaration of Competing Interest

Done

Acknowledgements

The first author would like to express his sincere gratitude to Fundação para a Ciência e Tecnologia (FCT) under the strategic project UIDB/EMS/00667/2020 for providing the partial funding of this work.

References

[1] Y. Hong, Fatigue and Fracture of the FRP-Wood Interface: Experimental Characterization and Performance Limits. Electronic Theses and Dissertations, The University of Maine, 2003.
[2] J.R. Correia, Adhesively Bonded Connections Between GFRP Pultruded Profiles in GFRP Pultruded Profiles in Civil Engineering, in: Adhesively Bonded Connections Between GFRP Pultruded Profiles in GFRP Pultruded Profiles in Civil Engineering, 4, Instituto Superior Técnico, 2008, pp. 161–231.
[3] H. Biscaia, R. Micaelo, C Chastre, Cyclic performance of adhesively bonded joints using the Distinct Element Method: damage and parametric analysis, Compos. Part B. 178 (2019) 107468.
[4] G.M. Raftery, A.M. Harte, P.D. Rodd, Bond quality at the FRP-wood interface using wood-laminating adhesives, Int. J. Adhes. Adhes. 29 (2) (2009) 101–110.
[5] J. Wan, Smith ST, P.Z. Qiao, FRP-to-softwood joints: an experimental investigation CICE2010, in: The 5th International Conference on FRP Composites in Civil Engineering, Beijing, China, 2010, pp. 27–29. September.
[6] G.M. Raftery, A.M. Harte, Low-grade glued laminated timber reinforced with FRP plate, Compos. Part B. 42 (4) (2011) 724–735.
[7] A.D. Jesus, J.M. Pinto, J.J. Morais, Analysis of solid wood beams strengthened with CFRP laminates of distinct lengths, Constr. Build. Mater. 35 (2012) 817–828.
[8] J. Wan, S.T. Smith, P. Qiao, F Chen, Experimental investigation on FRP-to-timber bonded interfaces, J. Compos. Constr. 18 (3) (2014) A4013006.
[9] J. Wan, S.T. Smith, P.Z. Qiao, in: FRP-to-softwood joints: Experimental investigation. Advances in FRP Composites in Civil Engineering, Springer, Berlin, Heidelberg, German, 2011, pp. 951–954.
[10] S.T. Smith, Strengthening of concrete, metallic and timber construction materials with FRP composites. CICE2010, in: The 5th International Conference on FRP Composites in Civil Engineering, Beijing, China, 2010, pp. 27–29. September.
[11] H.C. Biscaia, D. Cruz, C Chastre, Analysis of the debonding process of CFRP-to-timber interfaces, Constr. Build. Mater. 113 (2016) 96–112.
[12] H.C. Biscaia, C. Chastre, I.S. Borba, C. Silva, D Cruz, Experimental evaluation of bonding between CFRP laminates and different structural materials, J. Compos. Constr. 20 (3) (2016) 04015070.
[13] H. Biscaia, C. Chastre, D. Cruz, A Viegas, Prediction of the interfacial performance of CFRP laminates and old timber bonded joints with different strengthening techniques, Compos. Part B. 108 (2017) 1–17.
[14] H. Biscaia, P. Diogo, Experimental analysis of different anchorage solutions for laminated carbon fiber-reinforced polymers adhesively bonded to timber, Compos. Struct. 243 (2020) 112228.
[15] J. Wan, S.T. Smith, P. Qiao, F Chen, Experimental investigation on FRP-to-timber, J. Compos. Constr. 18 (3) (2014) A4013006.
[16] P. Diogo, Avaliação do Comportamento de Diferentes Soluções de Amarração de Compósitos de FRP em Elementos de Madeira, Nova University of Lisbon, 2020.
[17] H. Biscaia, C. Chastre, D. Cruz, N Franco, Flexural strengthening of old timber floors with laminated carbon fiber reinforced polymers, J. Compos. Constr. 20 (1) (2017) 04016073-1-20.
[18] H. Zhu, G. Wu, J. Shi, C. Liu, X He, Digital image correlation measurement of the bond-slip relationship between fiber-reinforced polymer sheets and concrete substrate, J. Reinf. Plast. Compos. 33 (17) (2014) 1590–1603.
[19] C. Yuan, W. Chen, Pham TM, H. Hao, Effect of aggregate size on bond behaviour between basalt fibre reinforced polymer sheets and concrete, Compos. Part B. 158 (2019) 459–474.
[20] C. Czaderski, K. Soudki, M Motavalli, Front and side view image correlation measurements on FRP to concrete pull-off bond tests, J. Compos. Constr. 14 (4) (2010) 451–463.
[21] E. Martinelli, C. Czaderski, M Motavalli, Modeling in-plane and out-of-plane displacement fields in pull-off tests on FRP strips, Eng. Struct. 33 (2011) 3715–3725.
[22] J.G. Dai, T. Ueda, Y. Sato, Development of the nonlinear bond stress-slip model of fiber reinforced plastics sheet-concrete interfaces with a simple method, J. Compos. Constr. 9 (1) (2005) 52–62.
[23] C. Carloni, K.V Subramaniam, FRP-masonry debonding: numerical and experimental study of the role of mortar joints, J. Compos. Constr. 16 (5) (2012) 581–589.
[24] B. Ghiassi, J. Xavier, D.V. Oliveira, P.B. Lourenço, Application of digital image correlation in investigating the bond between FRP and masonry, Compos. Struct. 106 (2013) 340–349.
[25] F.G. Carozzi, P. Colombi, C Poggi, Calibration of end-debonding strength model for FRP-reinforced masonry, Compos. Struct. 120 (2015) 366–377.
[26] M. Tekieli, S. De Santis, G. Felice, A. Kwiecień, F Roscini, Application of Digital Image Correlation to composite reinforcements testing, Compos. Struct. 60 (2017) 670–688.
[27] A. Kwiecień, P. Krajewski, Hojdys Ł, M. Tekieli, M Słoński, Flexible adhesive in composite-to-brick strengthening: experimental and numerical study, Polymers (Basel) 10 (4) (2018) 356.
[28] H.T. Wang, G. Wu, Y.T. Dai, X.Y. He, Determination of the bond-slip behavior of CFRP-to-steel bonded interfaces using digital image correlation, J. Reinf. Plast. Compos. 35 (18) (2016) 1–15.
[29] H.T. Wang, G. Wu, Y.T. Dai, X.Y. He, Experimental study on bond behavior between CFRP plates and steel substrates using Digital Image Correlation, J. Compos. Constr. 20 (6) (2016) 04016054.
[30] IPQ (Instituto Português da Qualidade)Madeiras - Ensaio Deflexão Estática b, NP 619, Lisbon, Portugal, 1973.
[31] IPQ (Instituto Português da Qualidade)Madeiras - Ensaio de Compressão Axial a, NP 618, Lisbon, Portugal, 1973.
[32] LNEC (National Laboratory of Civil Engineering)Especificação de Madeiras Para Estruturas, M1, Lisbon, Portugal, 1997.
[33] LNEC (National Laboratory of Civil Engineering)Madeira Para Construção, Casquinha. M4, Lisbon, Portugal, 1997.
[34] CEN (European Committee for Standardization)Eurocode 5: Design of Timber Structures - Part 1-1: General - Common Rules and Rules for Buildings, EN 1995-1-1, Brussels, Belgium, 2008.
[35] T. Carvalho, C. Chastre, H.C. Biscaia, R. Paula, Flexural behaviour of RC T-beams strengthened with diferent FRP materials, Presented at the 3rd fib International Congress – 2010, 2010.
[36] F. Mguil-Touchal S Morestin, M Brunei, in: Various Experimental Applications of Digital Image Correlation Method, 17, WIT Press, 1997, pp. 1–14.
[37] M. Palanca, G. Tozzi, L Cristofolini, The use of digital image correlation in the biomechanical area: a review, Int. Biomech. 3 (1) (2016) 1–21.
[38] G. Almeida, F. Melício, H. Biscaia, C. Chastre, J.M Fonseca, In-plane displacement and strain image analysis, Comput. Aided Civ. Infrastruct. Eng. 31 (4) (2016) 292–304.
[39] J. Górszczyk, K. Malicki, T Zych, Application of digital image correlation (DIC) method for road material testing, Materials (Basel) 12 (15) (2019) 2349.
[40] G.N. Eichhorn, A. Bowman, Haigh SK, S. Stanier, Low-cost digital image correlation and strain measurement for geotechnical applications, Strain (2020) e12348.
[41] H.C. Biscaia, N. Franco, C Chastre, Development of a simple bond-slip model for joints monitored with the DIC technique, Arch. Civil Mech. Eng. 18 (4) (2018) 1535–1546.
[42] H. Biscaia, N. Franco, C Chastre, Stainless steel bonded to concrete: an experimental assessment using the DIC technique, Int. J. Concrete Struct. Mater. 12 (2018) Article number: 9.
[43] GOM correlate software. 2020. Retrieved September 8 at http://www.gom.com/3d-software/gom-correlate.html.
[44] H. Biscaia, The influence of temperature variations on adhesively bonded structures: a non-linear theoretical perspective, Int. J. Non Linear Mech. 113 (2019) 67–85.
[45] H. Biscaia, Closed-form solutions for modelling the response of adhesively bonded joints under thermal loading through exponential softening laws, Mech. Mater. 148 (2020) 103527.
[46] D. Shen, X. Shi, Y. Ji, F Yin, Strain rate effect on bond stress-slip relationship between basalt fiber-reinforced polymer sheet and concrete, J. Reinf. Plast. Compos. 34 (7) (2015) 547–563.
[47] H.C. Biscaia, C. Chastre, C. Silva, C. Franco, Mechanical response of anchored FRP bonded joints: a nonlinear analytical approach, Mech. Adv. Mater. Struct. 25 (3) (2018) 238–252.
[48] T.G. Harmon, Y.J. Kim, J. Kardos, T. Johnson, A Stark, Bond of surface-mounted fiber-reinforced polymer reinforcement for concrete structures, ACI Struct. J. 100 (5) (2003) 557–564.
[49] A. Serbescu, M. Guadagnini, K Pilakoutas, Standardised double-shear test for determining bond of FRP to concrete and corresponding model development, Compos. Part B. 55 (2013) 277–297.
[50] S.Y. Seo, L. Feo, D Hui, Bond strength of near surface-mounted FRP plate for retrofit of concrete structures, Compos. Struct. 95 (2013) 719–727.
[51] D. Fernando, T. Yu, J Teng, Behavior of CFRP laminates bonded to a steel substrate using a ductile adhesive, J. Compos. Constr. 18 (2014) 04013040.
[52] Y.F. Wu, K. Liu, Characterization of mechanically enhanced FRP bonding system, J. Compos. Constr. 17 (1) (2013) 34–49.
[53] H.C. Biscaia, I.S. Borba, C. Silva, C Chastre, A nonlinear analytical model to predict the full-range debonding process of FRP-to-parent material interfaces free of any mechanical anchorage devices, Compos. Struct. 138 (2016) 52–63.
[54] J.G. Dai, T. Ueda, Y. Sato, Unified analytical approaches for determining shear bond characteristics of FRP-concrete interfaces through pullout tests, J. Adv. Concr. Technol. 4 (1) (2006) 133–145.
[55] F. Freddi, M Savoia, Analysis of FRP-concrete debonding via boundary integral equations, Eng. Fract. Mech. 75 (2008) 1666–1683.
[56] Y.W. Zhou, Y.F. Wu, Y Yun, Analytical modeling of the bond-slip relationship at FRP-concrete interfaces for adhesively-bonded joints, Compos. Part B. 41 (6) (2010) 423–433.
[57] K. Liu, Y.F. Wu, Analytical identification of bond-slip relationship of EB-FRP joints, Compos. Part B. 43 (4) (2012) 1955–1963.
[58] P. Carrara, D Ferretti, A finite-difference model with mixed interface laws for shear tests of FRP plates bonded to concrete, Compos. Part B. 54 (2013) 329–342.
[59] J. Pan, Y.F. Wu, Analytical modeling of bond behavior between FRP plate and concrete, Compos. Part B. 61 (2014) 17–25.
[60] Y. Yang, H. Biscaia, C. Chastre, M.A.G Silva, Bond characteristics of CFRP-to-steel joints, J. Constr. Steel Res. 138 (2017) 401–419.
[61] F. Focacci, A. Nanni, C.E Bakis, Local bond-slip relationship for FRP reinforcement in concrete, J. Compos. Constr. 4 (1) (2000) 24–31.
[62] H.C. Biscaia, C. Chastre, M.A.G Silva, Modelling GFRP-to-concrete joints with interface finite elements with rupture based on the Mohr-Coulomb criterion, Constr. Build. Mater. 47 (2013) 261–273.
[63] H. Ko, S. Matthys, A. Palmieri, Y Sato, Development of a simplified bond stress-slip model for bonded FRP-concrete interfaces, Constr. Build. Mater. 68 (2014) 142–157.

[64] F. Ascione, A. Napoli, R Realfonzo, Interface bond between frp systems and substrate: analytical modeling, Compos. Struct. (2020) 112942 in press.
[65] Z. Wu, H. Yuan, H. Niu, Stress transfer and fracture propagation in different kinds of adhesive joints, J. Eng. Mech. 128 (5) (2002) 562–573.
[66] J.G. Teng, H. Yuan, J.F Chen, FRP-to-concrete interfaces between two adjacent cracks: theoretical model for debonding failure, Int. J. Solids Struct. 43 (2006) 5750–5778.
[67] J. Wang, Debonding of FRP-plated reinforced concrete beam, a bond-slip analysis. I. Theoretical formulation, Int. J. Solids Struct. 43 (21) (2006) 6649–6664.
[68] Y.F. Wu, C. Jiang, Quantification of bond-slip relationship for externally bonded FRP-to-concrete joints, J. Compos. Constr. 17 (2013) 673–686.
[69] H.C. Biscaia, C. Chastre, M.A.G Silva, Bond-slip model for FRP-to-concrete bonded joints under external compression, Compos. Part B. 80 (2015) 246–259.
[70] P. Neto, J. Alfaiate, D. Dias-da-Costa, J Vinagre, Mixed-mode fracture and load misalignment on the assessment of FRP-concrete bond connections, Compos. Struct. 135 (2016) 49–60.
[71] M. Ghorbani, D. Mostofinejad, A Hosseini, Experimental investigation into bond behavior of FRP-to-concrete under mixed-mode I/II loading, Constr. Build. Mater. 132 (2017) 303–312.
[72] H.C. Biscaia, C. Chastre, M.A.G Silva, Nonlinear numerical analysis of the debonding failure process of FRP-to-concrete interfaces, Compos. Part B. 50 (2013) 210–223.
[73] A. Vahedian, R. Shrestha, K. Crews, Effective bond length and bond behaviour of FRP externally bonded to timber, Constr. Build. Mater. 151 (2017) 742–754.
[74] Biscaia H.C., Chastre C. and Viegas A. (2015). A new discrete method to model unidirectional FRP-to-parent material bonded joints subjected to mechanical loads.
[75] H. Biscaia, C. Chastre, Theoretical analysis of fracture in double overlap bonded joints with FRP composites and thin steel plates, Eng. Fract. Mech. 190 (2018) 435–460.
[76] J. Shi, H. Zhu, Z. Wu, R. Seracino, Bond behavior between basalt fiber-reinforced polymer sheet and concrete substrate under the coupled effects of freeze-thaw cycling and sustained load, J. Compos. Constr. 17 (4) (2013) 530–542.
[77] J. Vaculik, A.B. Sturm, P. Visintin, M.C Griffith, Modelling FRP-to-substrate joints using the bilinear bond-slip rule with allowance for friction: full-range analytical solutions for long and short bonded lengths, Int. J. Solids Struct. 135 (2018) 245–260.
[78] M. Zhu, T. Ueda, J.H. Zhu, Generalized evaluation of bond behavior of the externally bonded FRP reinforcement to concrete, J. Compos. Constr. 24 (6) (2020) 04020066.